Since January 2020 Elsevier has created a COVID-19 resource centre with free information in English and Mandarin on the novel coronavirus COVID-19. The COVID-19 resource centre is hosted on Elsevier Connect, the company's public news and information website.

Journal of Molecular Graphics and Modelling 108 (2021) 107997

Contents lists available at ScienceDirect

Journal of Molecular Graphics and Modelling

journal homepage: www.elsevier.com/locate/jmgm

Structure-based study of immune receptors as eligible binding targets of coronavirus SARS-CoV-2 spike protein

Saeed Mobini [a,1], Milad Chizari [b,1], Ladan Mafakher [c], Elmira Rismani [d], Elham Rismani [e,*]

[a] Department of Immunology, School of Public Health, Tehran University of Medical Sciences, Tehran, Iran
[b] Department of Medical Biotechnology, School of Allied Medical Sciences, Iran University of Medical Sciences, Tehran, Iran
[c] Thalassemia and Hemoglobinopathy Research Center, Health Research Institute, Ahvaz Jundishapur University of Medical Science, Ahvaz, Iran
[d] Payam Noor University, Biology Department, Tehran, Iran
[e] Molecular Medicine Department, Biotechnology Research Center, Pasteur Institute of Iran, Tehran, Iran

ARTICLE INFO

Keywords:
COVID-19
ACE2
SARS-CoV-2-binding receptors
Molecular docking
Homology modeling
Lymphopenia

ABSTRACT

One of the most important challenges in the battle against contagious SARS-CoV-2 is subtle identification of the virus pathogenesis. The broad range of COVID-19 clinical manifestations may indicate diversity of virus-host cells. Amongst key manifestations, especially in severe COVID-19 patients, reduction and/or exhaustion of lymphocytes, monocytes, basophils, and dendritic cells are seen.; therefore, it is required to recognize that how the virus infects the cells. Interestingly, angiotensin-converting enzyme 2 (ACE2) as the well-known receptor of SARS-CoV-2 is low or non-expressed in these cells. Using computational approach, several receptor candidates including leukocyte surface molecules and chemokine receptors that expressed in most lineages of immune cells were evaluated as the feasible receptor of spike receptor-binding domain (RBD) of SARS-CoV-2. The results revealed the higher binding affinity of CD26, CD2, CD56, CD7, CCR9, CD150, CD4, CD50, XCR1 and CD106 compared to ACE2. However, the modes of binding and amino acids involved in the interactions with the RBD domain of spike were various. Overall, the affinity of immune receptor candidates in binding to SARS-CoV-2 RBD may offer insight into the recognition of novel therapeutic targets in association with COVID-19.

1. Introduction

Severe acute respiratory syndrome coronavirus 2 (SARS-CoV-2) belongs to β-coronavirus genus causes zoonotic diseases, including the latest pandemic that has been emerged in the world. Positive single-stranded RNA SARS-CoV-2 virus has four main structural proteins include helical nucleocapsid protein (N), envelope glycoprotein (E), membrane glycoprotein (M), and spike glycoprotein (S) [1]. The virus RNA polymerase induces numerous of recombination. Continuous mutations have made the virus susceptible to transmission from animal to human and human to human [2]. Several of these mutations are D614G, N501Y and, P681H in the spike of the virus that is responsible for binding to its receptor, which has expanded the ability to infect and transmit the virus between humans [3–5].

Enveloped viruses mostly use multiple entry pathways, which can be divided into non-specific and specific bindings. Non-specific bindings aggregate viruses on the cell's surface, while specific bindings trigger proteins involved in endocytosis [6]. The viruses through non-specific bindings are attracted on the host cells glycosaminoglycans (Chondroitin and heparan-sulfate proteoglycans). Following initial bindings, the viruses by specific receptors are led to signaling cascades that stimulate endocytosis and are required for virus internalization. These incidents eventually spread infection to other cells and initiate the host immune responses [7]. It has been shown that spike glycoprotein of SARS-CoV-2 virus interacts with heparan sulfate and vimentin that facilitate binding of virus on the cells surface [8,9].

SARS-CoV-2 enters human cells through binding to transmembrane protein angiotensin-converting enzyme 2 (ACE2) as the well-known receptor [10]. Also, the virus requires proteases such as transmembrane protease serine 2 (TMPRSS2) and furin to cleave spike protein into S1 and S2 subunits to membrane fusion and internalization [11]. ACE2 is highly expressed in nasopharynx, oral mucosa, intestines, kidney, testis, and moderate in lung, heart, liver, vasculature, and low or none in nervous and immune systems [12,13].

SARS-CoV-2 disadjusts immune responses and leads to excessive

* Corresponding author.
E-mail addresses: elmirarismani7095@gmail.com (E. Rismani), el.rismani@gmail.com (E. Rismani).
[1] First co-author.

https://doi.org/10.1016/j.jmgm.2021.107997
Received 30 March 2021; Received in revised form 23 July 2021; Accepted 26 July 2021
Available online 28 July 2021

Abbreviations

Angiotensin-Converting Enzyme 2 (ACE-2)
Receptor-Binding Domain (RBD)
Severe Acute Respiratory Syndrome Coronavirus 2 (SARS-CoV-2)
Transmembrane Protease Serine 2 (TMPRSS2)
Monocyte Chemoattractant Protein-1 (MCP-1)
Cytokine Storm (CS)
Intensive Care Unit (ICU)
Acute Respiratory Distress Syndrome (ARDS)
Programmed Cell Death Protein 1 (PD-1)
T cell Immunoglobulin Mucin-3 (TIM-3)
Middle East respiratory syndrome (MERS)
Dipeptidyl Peptidase 4 (DPP4)
Protein Data Bank (PDB)
Iterative Threading ASSEmbly Refinement (I-TASSER)
Human Rhinoviruses (HRV)
Consensus Prediction Of Interface Residues in Transient complexes (CPORT)
Multiple Sequence Alignment (MSA)
Markov Cluster (MCL)
Cell Adhesion Molecules (CAMs)
Leukocyte Functional Ag-2 (LFA-2)
Super Immunoglobulin Family (SIgF)
Signaling Lymphocytic Activation Molecule (SLAM)
Intercellular Adhesion Molecule-1 (ICAM-1)
vascular cell adhesion molecule-1 (VCAM-1)
Neural Cell Adhesion Molecule (NCAM)
Neuropilin-1 (NRP1)
T Follicular Helper (TFH)

Table 1
Proteins in the study.

	Uniprot ID	PDB ID	Method	Resolution	R-value free	Organism
SARS-CoV-2-Spike	P0DTC2	6M0J.E.	X-RAY DIFFRACTION	2.45 Å	0.227	*Homo sapiens*
ACE2	Q9BYF1	6M0J.A.	X-RAY DIFFRACTION	2.45 Å	0.227	*Homo sapiens*
CCR5	P51681	6MEO.B	ELECTRON MICROSCOPY	3.90 Å	–	*Homo sapiens*
CCR9	P51686	5LWE.A	X-RAY DIFFRACTION	2.80 Å	0.243	*Homo sapiens*
CD4	P01730	5U1F.M	ELECTRON MICROSCOPY	6.80 Å	–	*Homo sapiens*
CD54-ICAM1	P05362	1Z7Z.I	ELECTRON MICROSCOPY	8.00 Å	–	*Homo sapiens*
CD26-DPP4	P27487	1WCY.A	X-RAY DIFFRACTION	2.20 Å	0.265	*Homo sapiens*
CD102-ICAM2	P13598	1ZXQ.A	X-RAY DIFFRACTION	2.20 Å	0.295	*Homo sapiens*
MERS-CoV-RBD	K9N5Q8	6L8Q.B	X-RAY DIFFRACTION	3.10 Å	0.241	MERS coronavirus
VP1, VP2, VP3	P03303	1K5M.ABC	X-RAY DIFFRACTION	2.70 Å	–	Rhinovirus B14

	Uniprot ID	**Template PDB**	**Sequence identity (%)**	**ProSA (Z-score)**	**I-Tasser (C-score)**	**Ramachandran plot quality (%)**			
						Most favored	**Additionally allowed**	**Generously allowed**	**disallowed**
CD150-SLAM	Q13291	1E07.A	28	−6.33	−3.37	77.9	13.8	4.8	3.4
CD2	P06729	1HNF.A	51	−5.11	−2.08	88.2	10.4	0.3	1.0
2B4-CD244	Q9BZW8	1E07.A	25	−4.38	−1.60	78.5	15.5	3.3	2.7
CD147-BSG	P35613	3B5H.A	47	−3.39	−0.47	83.8	12.9	1.8	1.5
CD7	P09564	5YFI.L	26	−5.14	−2.98	79.2	13.2	5.1	2.5
CD304-NRP1	O14786	4GZ9.A	91.5	−9.06	−2.67	87.3	11.9	0.4	0.4
CD56-NCAM	P13591	BIAA.A	24	−5.54	−0.69	77.0	17.7	2.8	2.5
CD50-ICAM3	P32942	1Z7Z.I	52	−7.56	−0.68	84.7	11.5	2.6	1.3
CD242-ICAM4	Q14773	4OIA.A	37	−4.38	0.57	89.8	9.7	0.0	0.5
CD106-VCAM	P19320	3DMK.A	23	−6.08	0.05	86.6	10.5	1.8	1.1
CXCR6	O00574	6WWZ.R	34	−2.47	−0.87	85.1	10.5	2.8	1.6
XCR1	P46094	5WB1.A	28	−2.26	−0.27	87.5	9.3	1.6	1.6

inflammatory responses. Reduced $CD4^+$ and CD8+T cells, NK, B cells (lymphopenia), monocytes, basophils and dendritic cells are vital experimental manifestations, especially in severe COVID-19 patients [14,15]. These reduced cell phenotypes were associated particularly with high IL-1β, TNF-α, IL-2, IL-6, IL-8, IL-10, IL-18, IFN-γ, IP-10 (CXCL-10), and MCP-1 serum levels (cytokine storm) (CS)) in those that required ICU [16–18]. CS can induce acute respiratory distress syndrome (ARDS) that results in alveolar collapse due to loss of surfactant, less oxygen entering the bloodstream and more fluid entering the alveolar [19–21].

Further, among T cells, a decrease in the memory T cell population (CD45RO +) has been shown that weaken COVID-19 patients' immune memory and predispose them to other diseases [22]. Likewise, T cells in patients with COVID-19 exhibit exhaustion phenotypes and PD-1 and TIM-3 levels are increased in the T cells subset. These functionally exhausted T cells may contribute to severe circumstances in COVID-19 patients [23].

Lymphopenia was also demonstrated in the Middle East respiratory syndrome (MERS) patients. MERS-CoV can directly infect human T lymphocytes and induce T-cell apoptosis via dipeptidyl peptidase 4 (DPP4 or CD 26), which is plenty found in lymphocytes [24]. There is a high homology between SARS-CoV-2, SARS-CoV, and MERS-CoV [25]. As lymphocytes do not express ACE2, it remains to be looked at whether novel receptors might mediate SARS-CoV-2 entry into T cells [26]. For this purpose, we computationally investigated several candidate receptors to predict possibility of SARS-CoV-2 virus entry to these cells. Briefly, the binding affinity and mode of interaction of immune receptors to the SARS-CoV-2 RBD were compared to ACE2 interactions

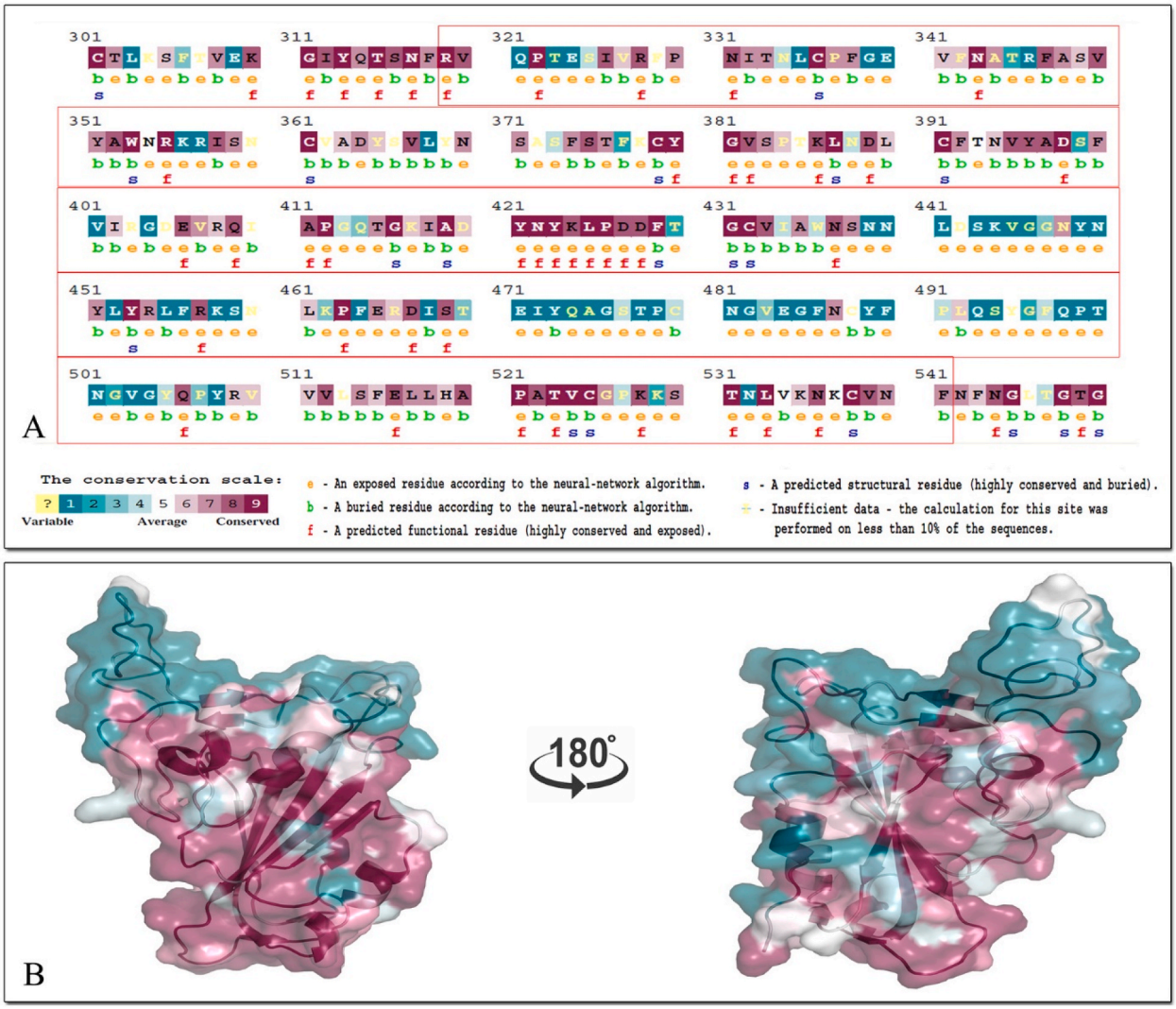

Fig. 1. A ConSurf analysis of SARS-CoV-2 spike. A) The sequence of RBD (319–541 in red box) that is colored by their conservation grades. (e: an exposed residue; b: a buried residue; f: a predicted functional residue; s: a predicte7d structural residue and yellow: insufficient data). B) The 3D structure of the RBD is presented using a space-cartoon model. The amino acids are colored by their conservation grades using the color-coding bar, with cyan-through-purple indicating variable-through-conserved. Positions, for which the inferred conservation level was assigned with low confidence, are marked with light yellow.

using homology modeling and molecular docking. One of the most advantages of this study is the identification of new candidate receptors that can be considered in novel therapeutic strategies.

2. Materials and methods

2.1. Sequences of proteins

To find the homologous structures of proteins, the retrieved amino acid sequences of proteins from Uniprot in canonical FASTA format were evaluated against Protein Data Bank (PDB) using NCBI Blast and HHpred (Table 1). HHpred performs the query-template alignment of proteins using PDB_mmCIF70 database [27].

2.2. Tertiary structure prediction and validation

Homology modeling was implemented as a comparative modeling method to build models of the 3D conformation of the proteins with no homologous structure. Using I-TASSER (Iterative Threading ASSEmbly Refinement), construction of full-length models started from multiple threading alignments to find structural templates from the PDB. Then, iterative fragment assembly simulations were followed by structure refinement to generate the 3D protein structures [28]. The PDB format of 2B4, CD2, CD7, CD50, CD106, CD147, CD150, CD242, CXCR6, XCR1 and NRP1 was obtained by uploading their amino acid sequence in FASTA format (Table 1). Eventually, the quality and reliability of the models were assessed by Protein Structure Analysis (ProSA) server and PROCHECK [29,30].

2.3. Identification of functional regions in SARS-CoV-2 spike

The biologically important regions of SARS-CoV-2 spike protein were evaluated using Consurf web server. To identify functional regions in protein, Consurf web server calculates the degree of conservation at each amino acid of protein based on the evolutionary relationships among the homologous sequences. Starting from either sequence or 3D structure, the server automatically collects homologues using multiple sequence alignment and reflects the evolutionary relations with color-code of cyan-through-purple in the range of 9 to 0 from highly conserved to the most variable [31,32]. The sequence of SARS-CoV-2 spike (Uniprot ID: P0DTC2) and the 3D structure of RBD (PDB ID: 6M0J.E.) were conducted to Consurf web server using the default parameters.

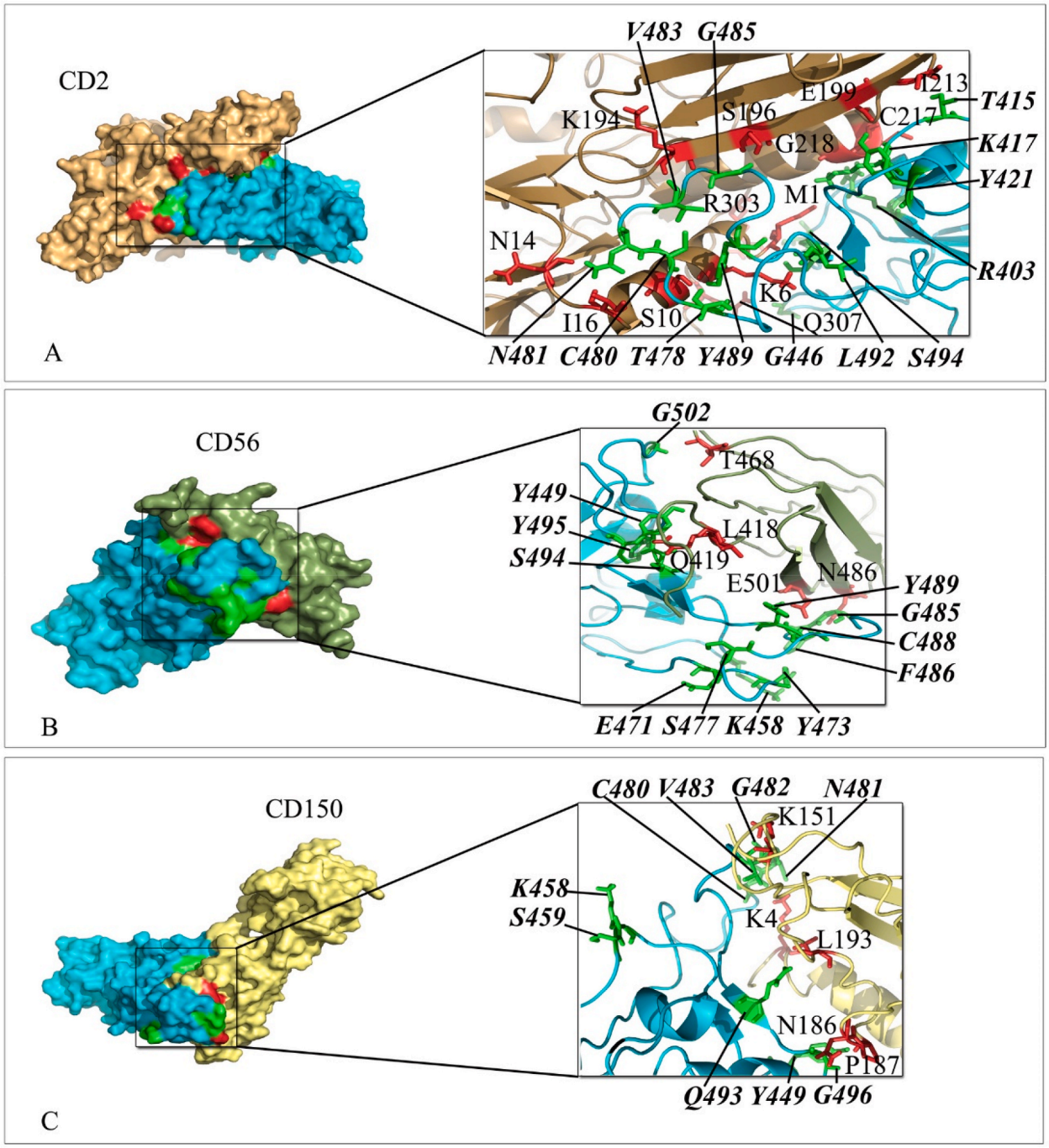

Fig. 2. Interaction mode of Ig-like domain of CD2, CD56 and CD150 with the RBD domain of SARS-CoV-2 spike. The surface representation of complexes that has resulted from molecular docking by HADDOCK. A) CD2/RBD-SARS-CoV-2, B) CD56/RBD-SARS-CoV-2 and C) CD150/RBD-SARS-CoV-2. RBD-SARS-CoV-2 is colored in cyan. Close-up view of the stick representation of amino acids (AA) involved in the interactions of proteins that are colored in red (inside the box) and green (bold-italic/outside) for receptors and RBD-SARS-CoV-2, respectively. (For interpretation of the references to color in this figure legend, the reader is referred to the Web version of this article.)

2.4. Molecular docking

The molecular interaction of protein-protein was explored by an information-driven flexible docking approach using HADDOCK and a rigid body docking by ClusPro webserver [33,34]. The 3D structure of proteins (either available PDBs or the predicted models) was uploaded as the first molecule (receptor) and the 3D structure of RBD of SARS-CoV-2 as the second one (ligand). Further, the molecular interaction of the Middle East respiratory syndrome (MERS) spike to CD26 and capsid proteins (VP1, VP2, VP3) of human rhinoviruses (HRV) to CD54 was evaluated to compare with the interactions of SARS-CoV-2 spike. The active residues of proteins were defined using CPORT (Consensus Prediction Of Interface Residues in Transient complexes) that predicts protein-protein interface residues [35]. Visualization and analysis of complexes of the top HADDOCK cluster was performed using PyMol and Ligplot + software, respectively [36,37]. The complexes with the lowest interaction energy and the highest interaction bonds (resulted from both docking webserver) were selected to calculate the binding affinity (ΔG) and dissociation constant (Kd) using PRODIGY server [38].

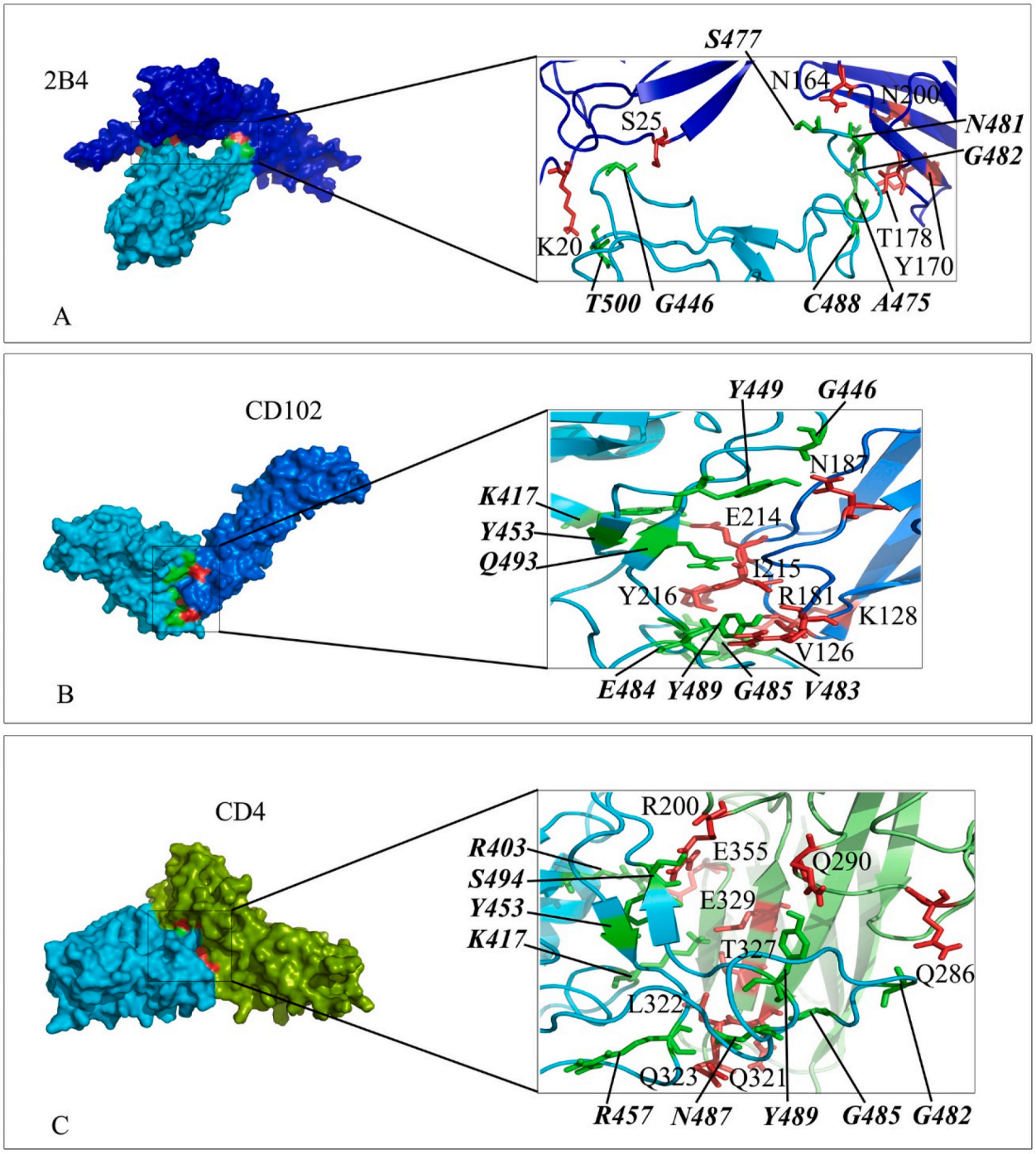

Fig. 3. Interaction mode of Ig-like domain of 2B4, CD102 and CD4 with the RBD domain of SARS-CoV-2 spike. The surface representation of complexes that has resulted from molecular docking by HADDOCK. A) 2B4/RBD-SARS-CoV-2, B) CD102/RBD-Sars-CoV-2 and C) CD4/RBD-SARS-CoV-2. RBD-SARS-CoV-2 is colored in cyan. Close-up view of the stick representation of amino acids (AA) involved in the interactions of proteins that are colored in red (inside the box) and green (bold-italic/outside) for receptors and RBD-SARS-CoV-2, respectively. (For interpretation of the references to color in this figure legend, the reader is referred to the Web version of this article.)

2.5. Molecular dynamics simulation

The molecular dynamics simulations (MD) were implemented for 12 complexes in the study using GROMACS version 2020.3 with the AMBER99SB-ILDN force field on a system accelerated with NVIDIA GPU [39]. System preparation was performed by solvation of proteins with SPC/E (extended simple point charge) water model in a cubic box of 10 Å marginal radius. The system ionization and neutralization were made with Na^+ and Cl^- ions. Energy minimization of the system was performed using the steepest descent algorithm to remove any steric clashes. The system was equilibrated with a canonical ensemble of 500 ps of NVT ensemble (constant number of particles, volume, and temperature) at 300 K using the Berendsen thermostat, following an isothermal-isobaric NPT ensemble (constant number of particles, pressure, and temperature). Finally, MD simulation was run at 300 K for a period of 100 ns with 2 fs time step. The output trajectories were analyzed in terms of time-dependent behavior of the system by calculating the root mean square deviation (RMSD), root-mean-square

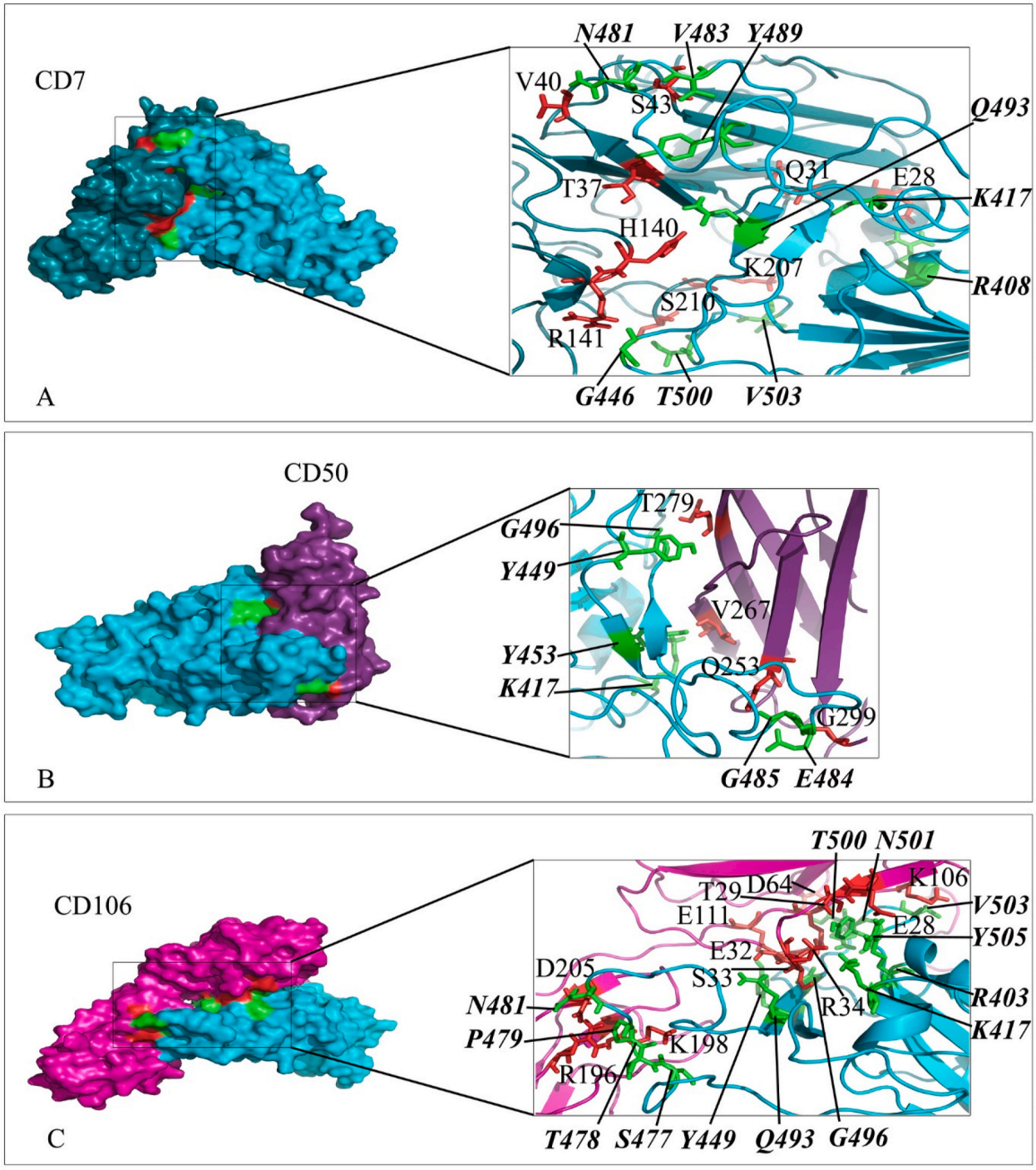

Fig. 4. Interaction mode of the extracellular domain of CD7, CD50 and CD106 with the RBD domain of SARS-CoV-2 spike. The surface representation of complexes that has resulted from molecular docking by HADDOCK. A) CD7/RBD-SARS-CoV-2, B) CD50/RBD-SARS-CoV-2 and C) CD106/RBD-SARS-CoV-2. RBD-SARS-CoV-2 is colored in cyan. Close-up view of the stick representation of amino acids (AA) involved in the interactions of proteins that are colored in red (inside the box) and green (bold-italic/outside) for receptors and RBD-SARS-CoV-2, respectively. (For interpretation of the references to color in this figure legend, the reader is referred to the Web version of this article.)

fluctuation (RMSF), radius of gyration (RoG), solvent accessible surface area (SASA) and hydrogen bonds (H-bonds). The graphs were visualized using GraphPad Prism version 8.4.3 for Windows.

2.6. Analysis of protein network

The biological information of protein–protein associations were collected using STRING database (Search Tool for Retrieval of Interacting Genes/Proteins) and Enrichr [40,41].

2.7. Multiple sequence alignment (MSA) and phylogenic study

To find conserved residues and regions in receptor proteins, Multiple Sequence Alignment (MSA) was carried out using Clustal Omega [42]. The reviewed sequences retrieved from Uniprot were subjected to MSA. The results of alignments were subjected to build the phylogenetic tree

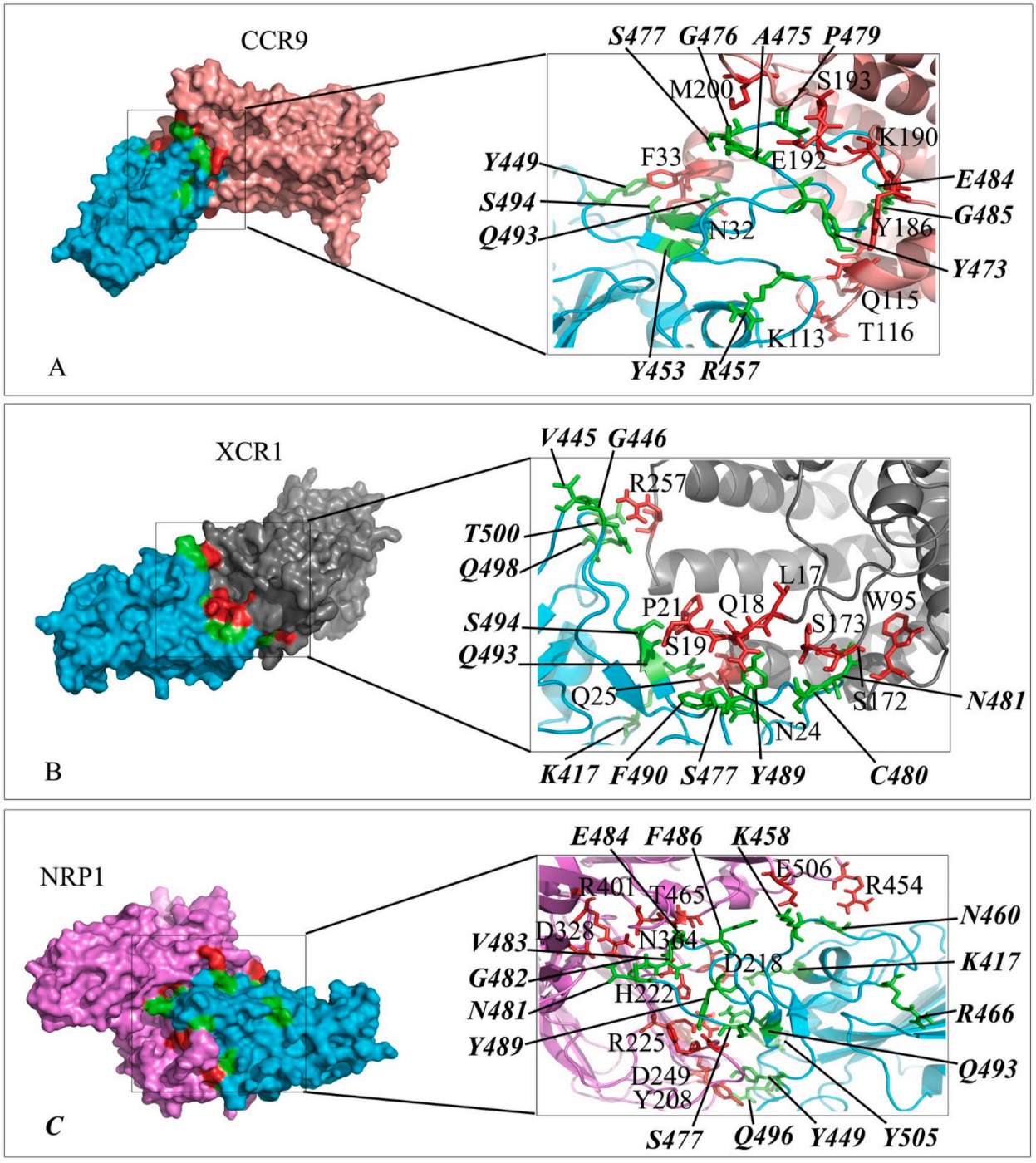

Fig. 5. Interaction mode of the extracellular domain of CCR9, XCR1 and NRP1 with the RBD domain of SARS-CoV-2 spike. The surface representation of complexes that has resulted from molecular docking by HADDOCK. A) CCR9/RBD-SARS-CoV-2, B) XCR1/RBD-SARS-CoV-2 and C) NRP1/RBD-SARS-CoV-2. RBD-SARS-CoV-2 is colored in cyan. Close-up view of the stick representation of amino acids (AA) involved in the interactions of proteins that are colored in red (inside the box) and green (bold-italic/outside) for receptors and RBD-SARS-CoV-2, respectively. (For interpretation of the references to color in this figure legend, the reader is referred to the Web version of this article.)

using MEGA7 [43].

3. Results

3.1. 3D structure of proteins

The sequence-template alignment using Blastp and HHpred resulted in finding 3D structure of SARS-CoV-2 RBD, ACE2, CCR5, CCR9, CD4, CD54, CD26, CD102, MERS-CoV-RBD, VP1, VP2 and VP3 of rhinovirus in PDB (6M0J.E., 6M0J.A., 6MEO.B, 5LWE.A., 5U1F.M., 1Z7Z.I., 1WCY.A, 1ZXQ.A, 6L8Q.B, 1K5M.A, 1K5M.B and 1K5M.C, respectively) (Table 1).

3.2. Homology modeling of the proteins

The five top models of 3D structure predicted by I-TASSER for each sequence were ranked by C-scores ranging from−5 to 2. The one with the highest C-score was selected as the best model for further analysis

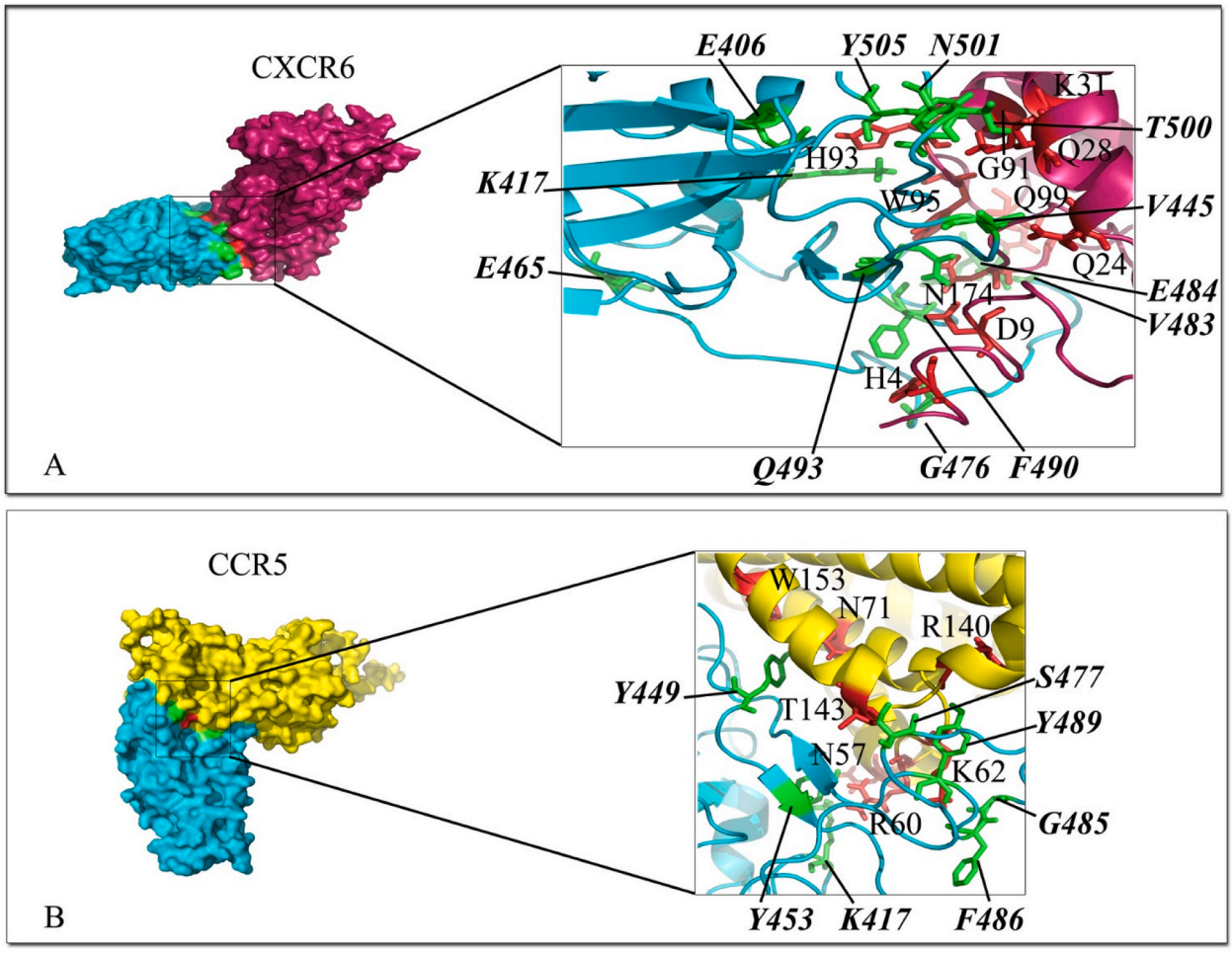

Fig. 6. Interaction mode of the extracellular domain of CXCR6 and CCR5 with the RBD domain of SARS-CoV-2 spike. The surface representation of complexes that has resulted from molecular docking by HADDOCK. A) CXCR6/RBD-SARS-CoV-2, and B) CCR5/RBD-SARS-CoV-2. RBD-SARS-CoV-2 is colored in cyan. Close-up view of the stick representation of amino acids (AA) involved in the interactions of proteins that are colored in red (inside the box) and green (bold-italic/outside) for receptors and RBD-SARS-CoV-2, respectively. (For interpretation of the references to color in this figure legend, the reader is referred to the Web version of this article.)

(data in Table 1). Firstly, there was a convenient consistency between the predicted structure and the secondary structure prediction. Secondly, the stereochemical features of the predicted structures were assessed using PROCHECK, and ProSA servers. Data are summarized in Table 1. ProSA Z-score for each protein indicated the overall model quality by evaluating the conformity of the models with the experimentally determined protein chains. Analysis of Ramachandran plot of the 3D structures from PROCHECK indicated that an acceptable percentage of the residues could be detected in the most favored areas of plot and allowed regions of it.

3.3. Evolutionary analysis of the sequence and 3D structure of SARS-CoV-2 spike

In ConSurf, the evolutionary rate of sequence and 3D structure of SARS-CoV-2 spike was estimated based on a specified probabilistic model of amino-acid substitutions. The conservation scores calculated by ConSurf were depicted in a coloring scheme indicating the relative measure of evolutionary conservation at each sequence site. The analysis revealed the functional (f), exposed (e), structural (s) and buried (b) residues of the protein. There are number of functional (highly conserved and exposed) and structural residues in the RBD of spike (319–541), where they are depicted by their conservation grades. The sequence analysis of SARS-CoV-2 spike (including RBD) and the colored protein structure (generated by PyMol) are shown in Fig. 1.

3.4. Comparable interaction of receptors and SARS-CoV-2 spike in the complexes

The interaction mode of receptors and SARS-CoV-2 spike was studied using HADDOCK webserver. The following active interface amino acid residues: K417, Y421, G446, Y449, Y453, L455, F456, R457, K458, S459, E471, I472, Y473, Q474, A475, G476, S477, T478, P479, C480, N481, G482, V483, E484, G485, F486, N487, C488, Y489, F490, Q493, G496, Q498, T500, G502 and Y505 from the RBD domain of SARS-CoV-2 spike protein were defined to drive molecular docking. The top-ranking pose for docked complexes were selected from HADDOCK clusters with the lowest total intermolecular energies (Kcal/mol) and the least average pairwise backbone RMSD (Å) at their interface. The results including interacting residues of either Ig-like domain or extracellular domain of receptors and residues of RBD domain of SARS-CoV-2 spike are depicted in Figs. 2–9. Further, the number of hydrogen bonds, free energy of binding and the dissociation constant (Kd) value of complexes are summarized in Table 2.

3.5. The dynamics of proteins/RBD-spike interactions

Considering the results in Table 2, the 12 proteins/RBD-spike

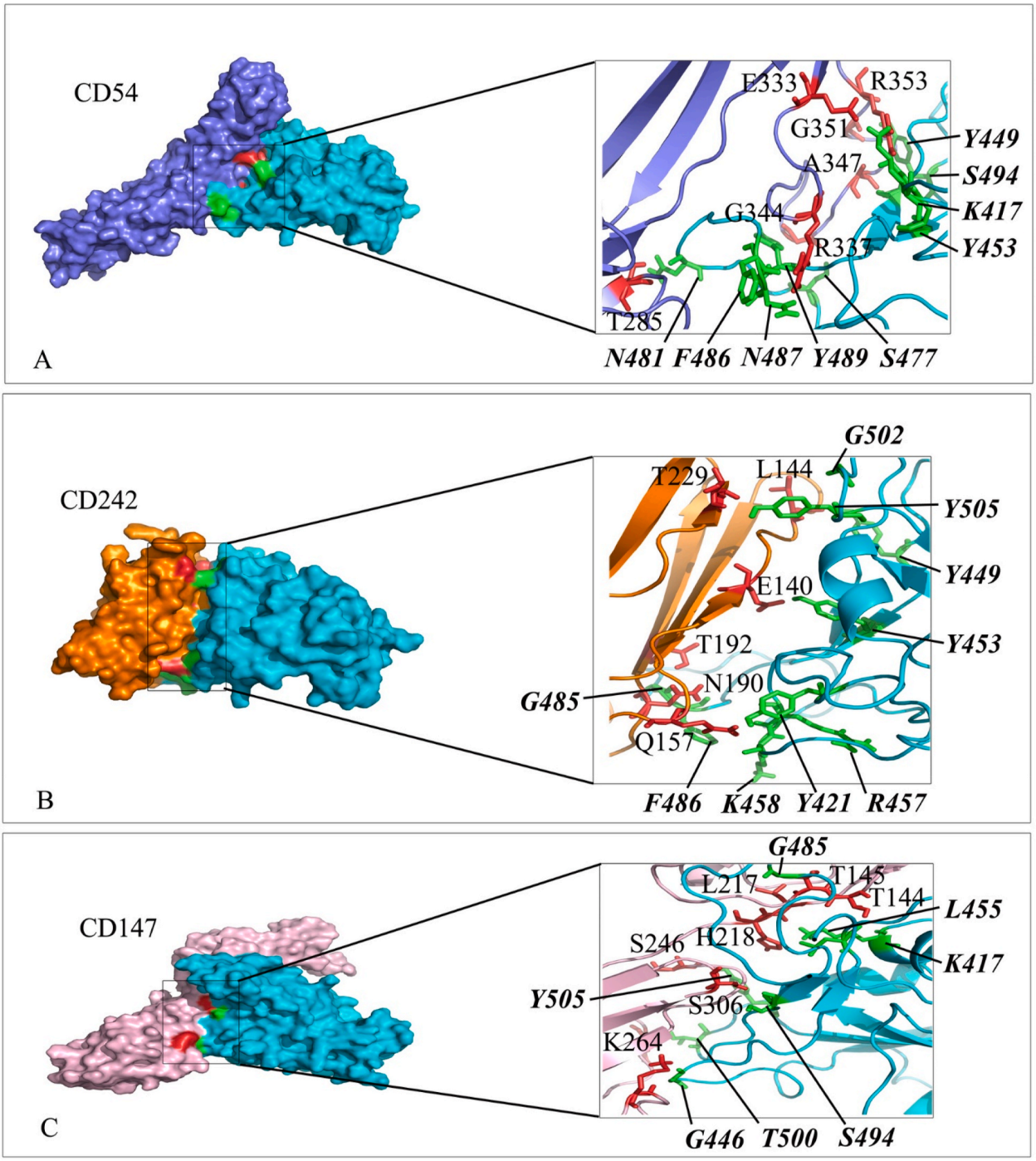

Fig. 7. Interaction mode of the extracellular domain of CD54, CD242 and CD147 with the RBD domain of SARS-CoV-2 spike. The surface representation of complexes that has resulted from molecular docking by HADDOCK. A) CD54/RBD-SARS-CoV-2, B) CD242/RBD-SARS-CoV-2 and C) CD147/RBD-SARS-CoV-2. RBD-SARS-CoV-2 is colored in cyan. Close-up view of the stick representation of amino acids (AA) involved in the interactions of proteins that are colored in red (inside the box) and green (bold-italic/outside) for receptors and RBD-SARS-CoV-2, respectively. (For interpretation of the references to color in this figure legend, the reader is referred to the Web version of this article.)

complexes at the top of the table were subjected to 100ns MD simulations using the GROMACS package. The MD trajectories were analyzed in terms of root mean square deviation (RMSD) of the structures during simulations. RMSD plots are depicted in Fig. 10. A. While the lowest fluctuations were related to CD4ɜ CD26, and XCR1 complexes, the RMSD of the complexes was in the range of 0.2–1 nm and showed the steady states at the final time of simulations.

Furthermore, the average fluctuation of each residue during the simulation was calculated as the root mean square fluctuation (RMSF) of the CA atoms. The results were plotted for each complex to display residue fluctuations of RBD-spike (Fig. 10B). Analysis of RMSFs pattern revealed that the RBD-spike residues in the complexes had relatively similar fluctuations in the range of 0.05–0.3 nm (except for the C-terminal residues of RBD-spike with higher fluctuation up to 0.45 nm). The average fluctuation of each residue of CD26 in complex with either RBD-spike of SARS-CoV-2 or MERS was evaluated during the simulation. The RMSF pattern of residues in the interface of CD26 (240–440) indicated different residue fluctuations (Fig. 11A), where CD26 residues in

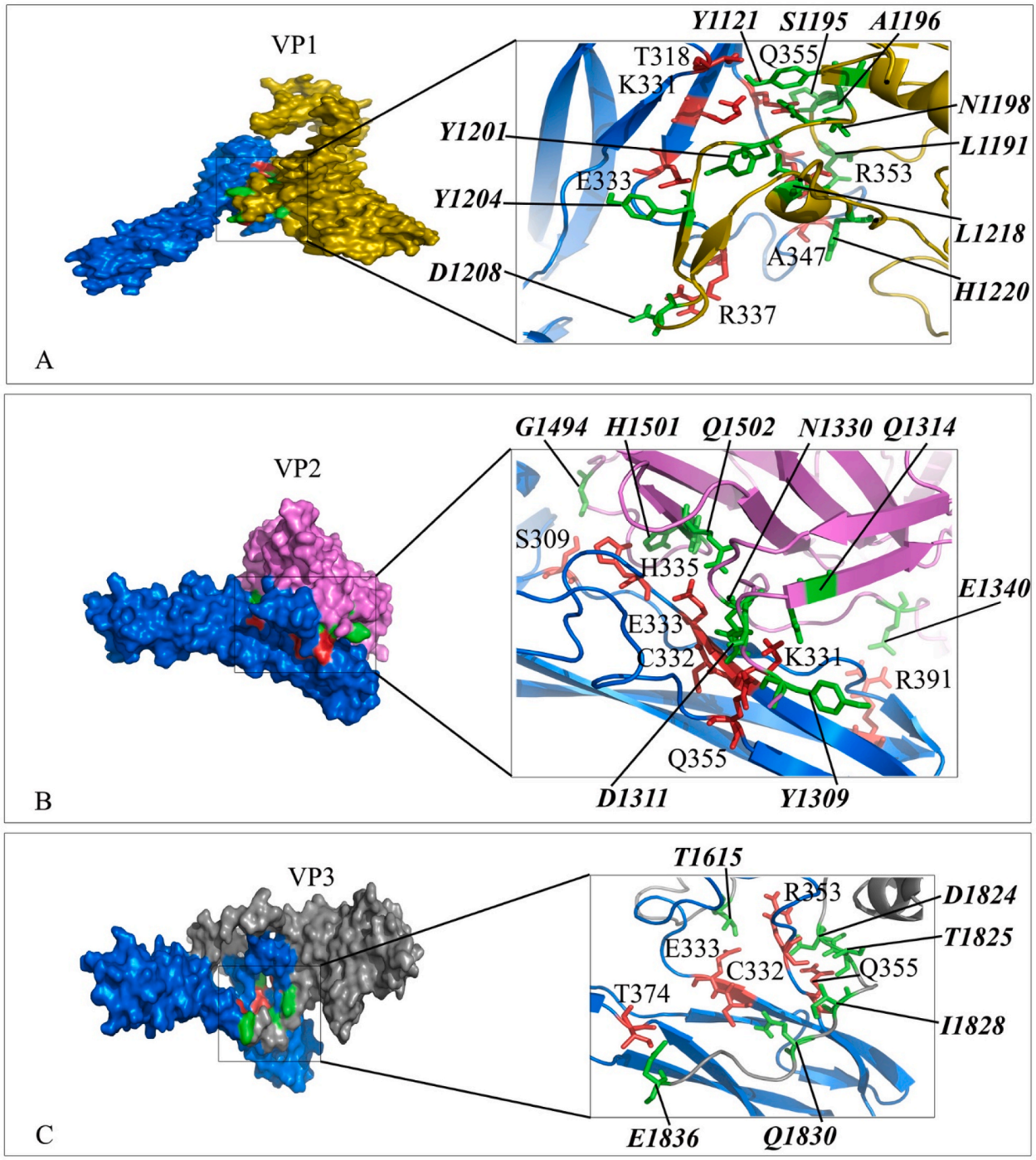

Fig. 8. Interaction mode of the extracellular domain of CD54 with the domain of VP1, VP2 and VP3 of Rhinovirus. The surface representation of complexes that has resulted from molecular docking by HADDOCK. A) CD54/VP1, B) CD54/VP2 and C) CD54/VP3. CD54 is colored in blue. Close-up view of the stick representation of amino acids (AA) involved in the interactions of proteins that are colored in red (inside the box) and green (bold-italic/outside) for receptors and VPs, respectively. (For interpretation of the references to color in this figure legend, the reader is referred to the Web version of this article.)

complex with MERS showed higher fluctuations. Fluctuations in the RMSF plot of the CD26/RBD-spike ranged from 0.1 to 0.4 nm and in the CD26/MERS plot ranged from 0.01 to 0.7 nm.

The radius of gyration determines the protein structure compactness, the higher values throughout the protein size range describe a less tight packing, whereas the lower radius of gyration indicates the tighter packing of proteins. While the compression fluctuations of the complexes during the simulation are limited, the lowest compactness was related to the CD56/RBD-spike complex with RoG of 2 nm and the other complexes showed RoG in the range of 2.4–3.2 nm (Fig. 11B).

The density of hydrogen bonds between two different proteins at an interface plays a significant role in joining two different proteins together. Number of H-bonds at the interface of proteins and RBD-spike were plotted during the simulation that showed diverse range of less than 5 to more than 20 H-bonds. The distribution of amino acid composition at the protein–protein interfaces and the difference of amino acid side chains resulted in varying number of interactions. There was a relatively well agreement between number of H-bonds after

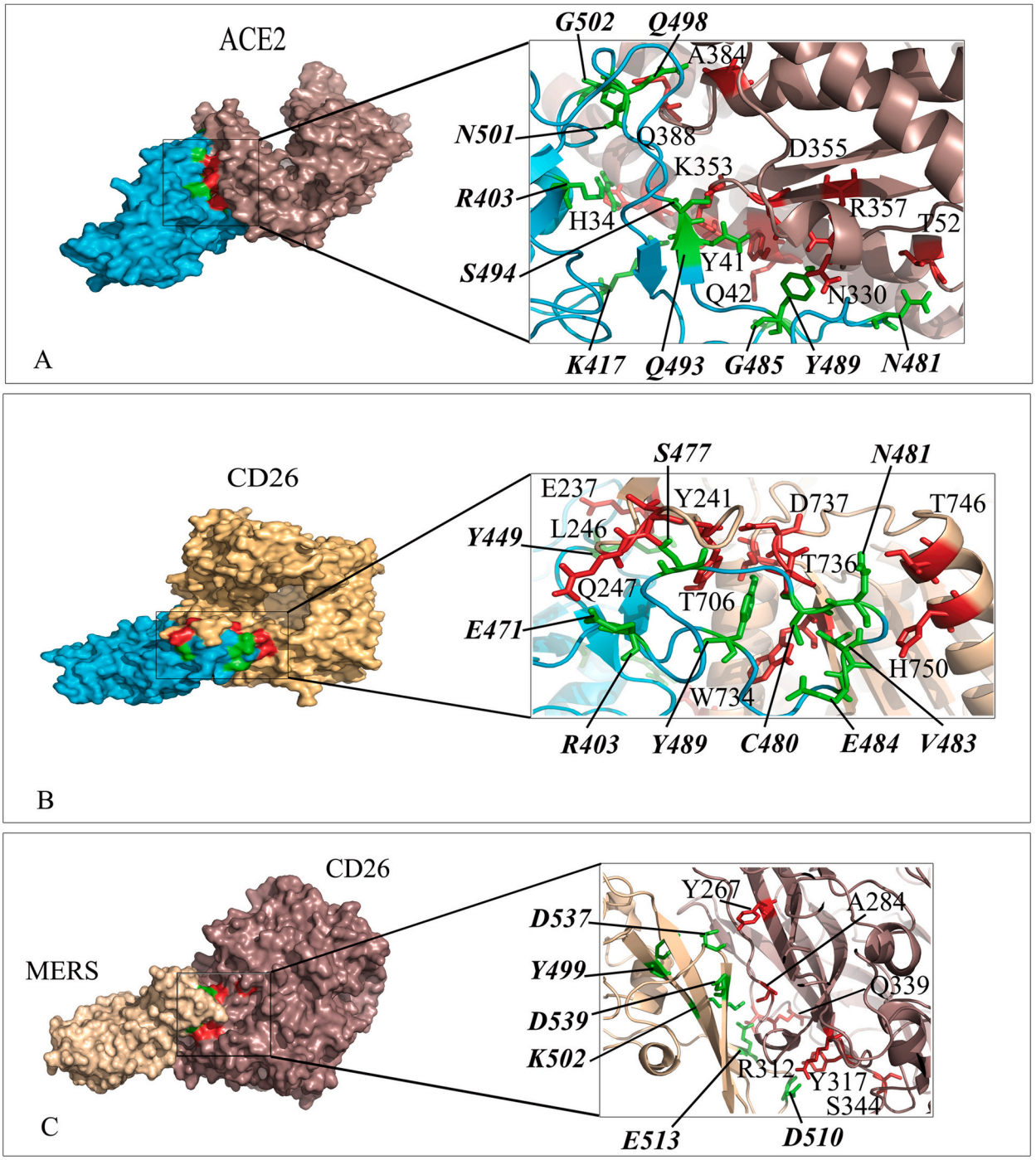

Fig. 9. Interaction mode of the extracellular domain of CD26 and ACE2 with the RBD domain of SARS-CoV-2 spike as well as CD26 with MERS. The surface representation of complexes that has resulted from molecular docking by HADDOCK. A) ACE2/RBD-SARS-CoV-2, B) CD26/RBD-SARS-CoV-2 and C) CD26/MERS. RBD-SARS-CoV-2 and MERS are colored in cyan and wheat. Close-up view of the stick representation of amino acids (AA) involved in the interactions of proteins that are colored in red (inside the box) and green (bold-italic/outside) for receptors and RBD-SARS-CoV-2/MERS, respectively. (For interpretation of the references to color in this figure legend, the reader is referred to the Web version of this article.)

molecular docking and molecular dynamic simulation analysis (Table 3, Fig. 11C).

The solvent accessible surface area (SASA) was computed for the interface of proteins and RBD-spike to evaluate desolvation of the protein cavity and their binding affinity. Higher SASA values are defined as more exposed amino acids into solvent, whereas, lower scores indicate more buried residues in the protein. The SASA plot analysis revealed that complexes are classified in three range of SASA: ACE2/RBD-spike and CD56/RBD-spike showed the highest value (60–70 nm^2), CD26/MERS had SASA around 50 nm^2 and the other complexes were in the range of 35–45 nm^2 (Fig. 11D).

3.6. Protein-protein interaction network and KEGG enrichment analysis of human receptors

Interacting residues of the RBD domain of SARS-Cov-2 spike into residues of receptors were mapped to find the most common residues of the RBD domain (Fig. 12A). CD2 and NRP1 had the highest number of

Table 2
Molecular docking results of complexes.

Complexes	HADDOCK energy (Kcal/mol)	PRODIGY		ClusPro		PRODIGY	
		ΔG (Kcal/mol)	Kd (M) at 37.0 ◦C	Cluster Members	Lowest Energy (Weighted Score)	ΔG (Kcal/mol)	Kd (M) at 37.0 ◦C
CD26/RBD-spike	−339.4	−16.3	3.40E-11	223	−3512.6	−16.5	2.10E-12
CD26/RBD-MERS	−321.7	−11.1	1.60E-09	152	−1923.9	−13.6	2.40E-10
CD2/RBD-spike	−319.6	−16.2	3.70E-11	105	−2892.6	−17.3	6.80E-12
CD56/RBD-spike	−310	−15.1	2.10E-11	143	−2960.5	−14.3	8.00E-11
CD7/RBD-spike	−349.2	−15	2.60E-11	238	−3804.3	−14.2	1.00E-11
CCR9/RBD-spike	−329.9	−14.2	9.40E-11	253	−4031.5	−15.3	2.60E-12
CD150/RBD-spike	−337	−13.7	2.30E-10	219	−3266.8	−14.2	9.10E-11
CD4/RBD-spike	−295.2	−13.3	4.50E-10	185	−2092.4	−18.6	8.00E-10
CD50/RBD-spike	−272.6	−13.2	4.60E-10	177	−2407.2	−13.4	3.40E-10
XCR1/RBD-spike	−314	−13.1	5.80E-10	212	−3317.5	−18	1.90E-11
CD106/RBD-spike	−351.9	−12.9	7.70E-10	399	−4642.8	−14	1.30E-10
ACE2/RBD-spike	−393.6	−12.8	8.80E-10	358	−4587.4	−13.6	1.00E-11
CD54/RBD-spike	−248.5	−12.8	9.00E-10	186	−1952.3	−14.7	4.30E-10
CD54/VP1	−386.2	−12.6	1.40E-09	49	−1759.1	−16.7	1.60E-10
CD54/VP2	−240.1	−13.3	4.40E-10	93	−1882.1	−14.3	8.30E-10
CD54/VP3	−340.9	−13.7	2.00E-10	80	−2631.4	−16.2	3.60E-10
NRP1/RBD-spike	−382.3	−12.7	1.10E-09	216	−2682	−13.9	1.50E-10
CD242/RBD-spike	293.6	−12.6	1.40E-09	178	−2005.5	−12.7	1.00E-09
CCR5/RBD-spike	−222.8	−12.5	1.50E-09	87	−2433.2	−12	3.70E-09
CXCR6/RBD-spike	−330.1	−12.4	1.90E-09	93	−2599.2	−13.5	4.60E-10
CD147/RBD-spike	−235.9	−11.9	4.40E-09	145	−2488.1	−13.3	4.30E-10
CD102/RBD-spike	−275.5	−11.6	6.40E-09	298	−2766.9	−10.6	9.40E-10
2B4/RBD-spike	−202.5	−11.5	7.50E-09	146	−2496.6	−11.4	8.90E-09

interacting residues, though their interaction pattern was different. Interestingly, the variable and less protected amino acids of the RBD domain of spike were among the common amino acids involved in the interaction with the receptors rather than the more conserved amino acids. For example, K417, G446, Y449, S477, N481 and G485, which are less conserved, co-interact with the most receptors.

The full STRING network with a medium FDR stringency of 5 % and a medium confidence cutoff of 0.4 was created to find PPI network of above-mentioned receptors (Fig. 12B). STRING database predicted the functional interaction pattern of proteins. By applying the Markov Cluster algorithm (MCL) as clustering method (default: 3), proteins separated as DPP4 and ACE2 together, ICAM1-4, VCAM1, XCR1 and BSG in the next cluster and NRP1, NCAM1, CD244, SLAMF1, CD7, CD2, CD4, CCR5, CCR9 and CXCR6 in the third cluster. The experimentally interaction is predicted for CD4/CCR5 and CD4/CD2 (magenta line), whereas, the remaining partners showed text mining association in the form of light-yellow lines.

KEGG analysis revealed that the receptors were enriched in ten pathways including, Cytokine-cytokine receptor interaction, Chemokine signaling pathway, Hematopoietic cell lineage, Cell adhesion molecules (CAMs), Human immunodeficiency virus1 infection, Human T-cell leukemia virus1 infection, Renin-angiotensin system, Primary immunodeficiency, Intestinal immune network for IgA production and Antigen processing and presentation. The terms in which the receptors were enriched and ordered by p-value are listed in Fig. 12. C.

To trace evolutionary relation of proteins in terms of common domains, the receptor protein sequences were aligned and compared based on Neighbor Joining method with bootstrapping to provide confidence for tree topology (Fig. 12D). The percentage of replicate trees in which the associated taxa clustered together in the bootstrap values (1000 replicates) has been depicted next to the branches. Proteins in a common family (ICAM2/4 and ICAM1/3) showed higher score, no close and high-score evolutionary relationship was observed between receptor sequences.

4. Discussion

SARS-CoV-2 infection can result in a considerable reduction in circulating lymphocytes, NK, monocytes, basophils and dendritic cells, and proper immune potential in both severe and moderate patients. One reason for this reduction may be due to the direct entry of the virus into the cells. This infectivity occurs through the surface receptors of these cells such as ACE-2. Paradoxically, ACE-2 is not thoroughly expressed in the cells, the question remains to be answered whether other receptors are involved in virus entry [44]. To answer this question, we evaluated a number of candidate receptors that could facilitate virus entry into the cell.

Since the dominant technique that was implemented to evaluate the protein-protein interactions was molecular docking, there is a need to validate the docking programs. A common method for validation of the docking programs is re-docking the components of a known conformation and comparing to the co-crystallized structure. A program that results in returning the poses below an acceptable Root Mean Square Deviation (RMSD) value from the known conformation (usually 1.5 or 2 Å) is considered a successful docking program [45]. Likewise, RMSD of re-docking conformation of ACE2/spike from PDB: 6M0J and CD26/MERS from PDB: 6L8Q with both docking programs were calculated using align option in PyMol software. The RMSD of ACE2/spike complexes of HADDOCK and ClusPro aligned to 6M0J and CD26/MERS complexes aligned to 6L8Q were 0.921, 0.996, 0.908 and 0.942, respectively. Likewise, there was a well accordance in the results of complexes of both programs when evaluated in terms of the binding affinity and dissociation constant by PRODIGY.

In our study, CD26, which is the well-known receptor of the MERS-CoV virus and plays an important role in lymphocyte infection [24], has the strongest interaction with the SARS-CoV-2 virus spike. CD26 or dipeptidyl peptidase-4 (DPP4) is identified as a co-stimulator for T cell activation and expressed on T cell and also B cell, macrophages, NK, and thymocytes [46–48]. In consistent with the results of Li et al. that

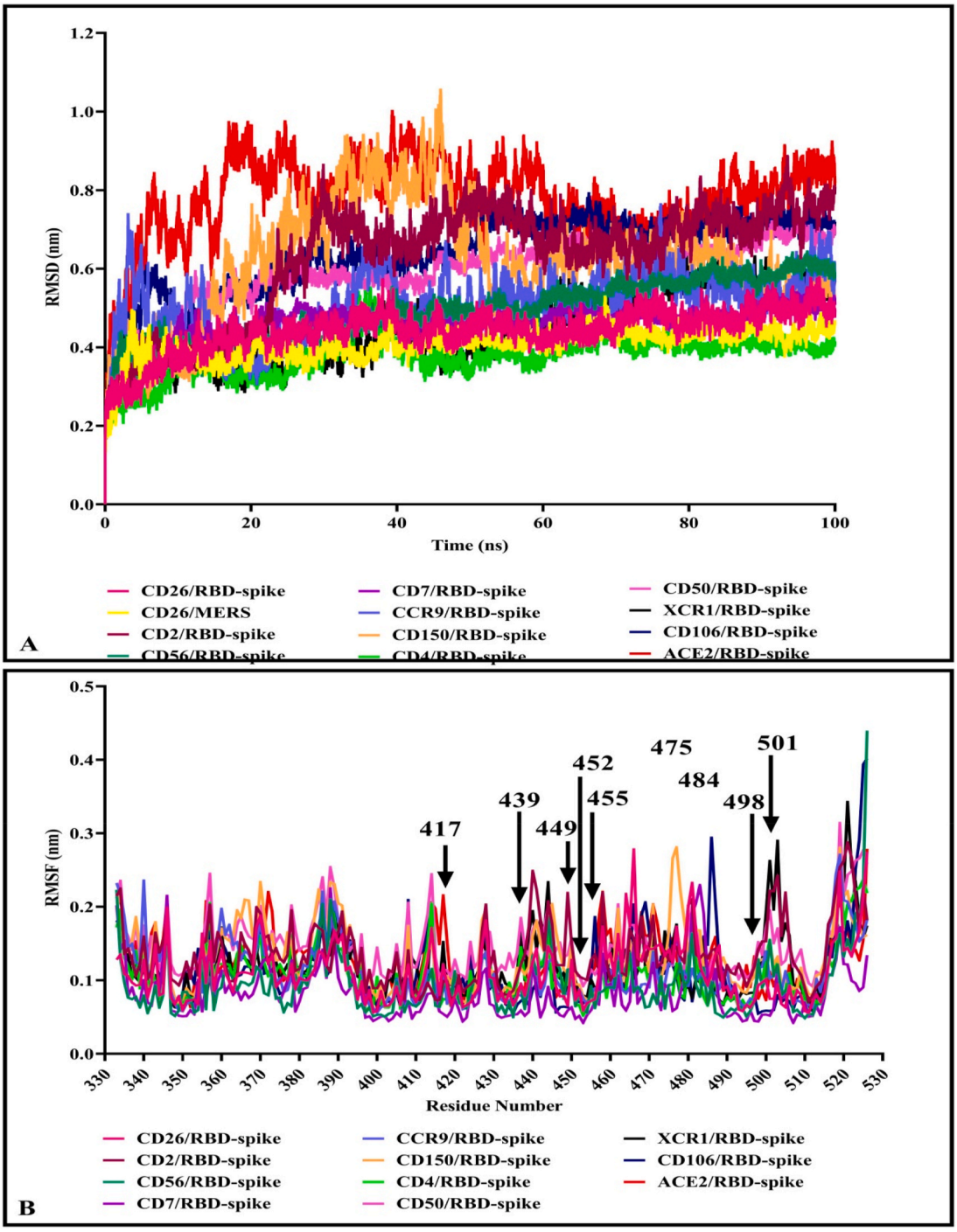

Fig. 10. RMSD and RMSF plot of the complexes after 100 ns by MD simulations. A) RMSD of the backbone atoms of protein/RBD-spike complexes that showed finally the systems appeared to reach equilibrium after 100 ns. B) The RMSF plots of RBD-spike in complexes. Key residues of RBD-spike are depicted by arrow.

reported almost identical binding pattern of SARS-CoV-2-S RBD and MERS-CoV-S RBD with DPP4 using ZDOCK [49], HADDOCK outputs revealed the CD26 residues K267, R336, R317, and Q344 contributed significantly in the interaction with both RBDs. However, the binding affinity resulted from both molecular docking programs showed higher affinity of CD26/RBD-SARS-CoV-2 compared to MERS-CoV-S RBD/CD26.

It is proposed that cell adhesion molecules could be convenient candidates for virus binding considering weak physiological ligand binding affinities compared to the stronger virus binding affinity for the receptor [50]. CD2 or leukocyte functional Ag-2 (LFA-2) is an integral glycoprotein and a member of the super immunoglobulin family (SIgF) which is expressed on T, NK, NKT cells, and thymocytes. It acts as T cell adhesion molecule to target cell and antigen presenting cells, T cell activation, signal transduction, and regulation of cytolysis [51,52]. Other members of the CD2 family that could mention as potentially SARS-CoV-2 receptor include CD150 or signaling lymphocytic activation molecule (SLAM) and CD244 or 2B4 [53,54]. The binding affinity of CD2/spike was higher than ACE2/spike, though there was no current report of binding details of CD2 and spike. The SLAM receptor interacted with spike through immunoglobulin (Ig) domain and resulted in moderately higher binding affinity compared to ACE2/spike as

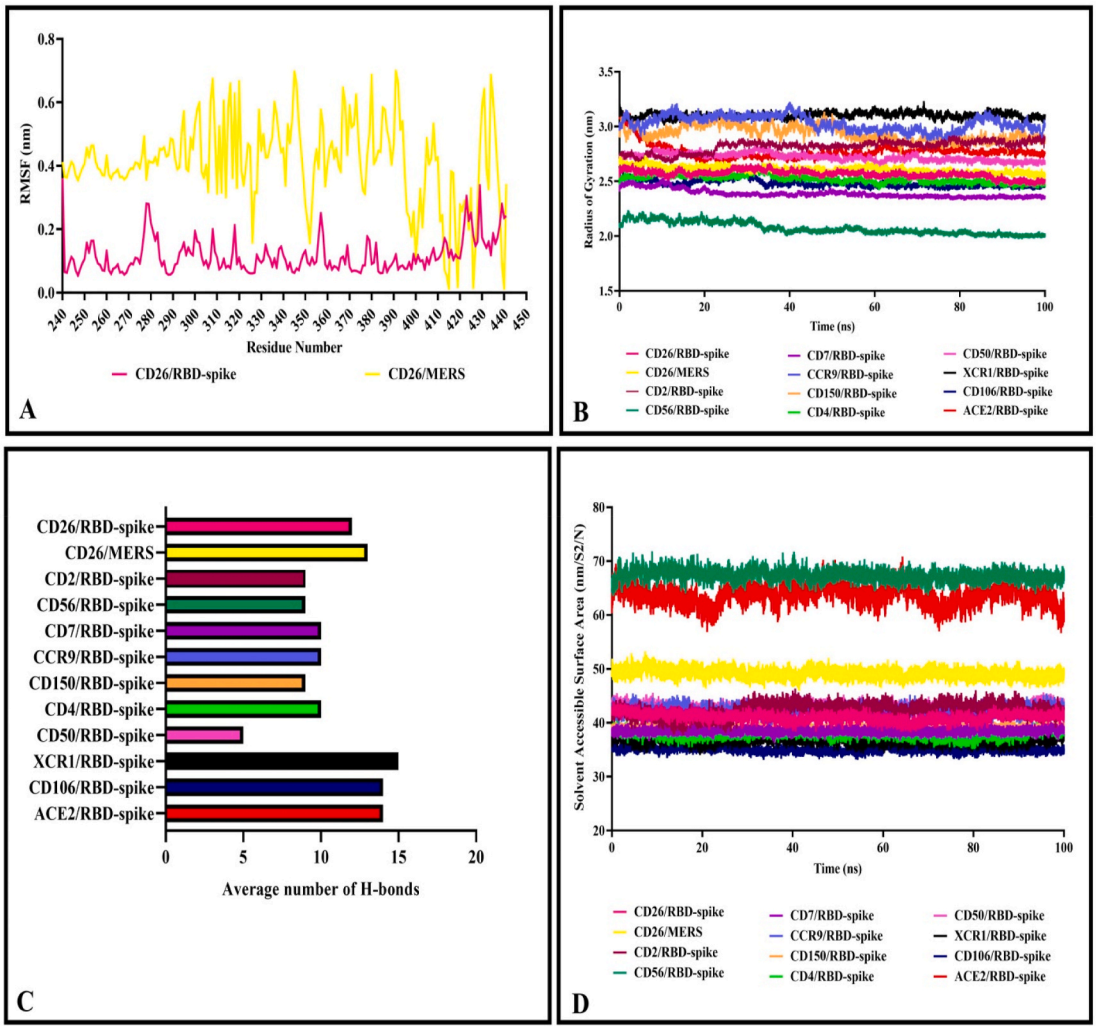

Fig. 11. RMSF, RoG, SASA, and H-bonds plot of the complexes after 100 ns by MD simulations. A) The RMSF plot of CD26 in complex with RBD-spike and MERS. B) Radius of gyration of complexes. C) The average number of H-bonds in the interface of proteins and RBD-spike. D) Solvent accessible surface area in the interface of proteins and RBD-spike.

cognitive SARS-CoV-2 RBD receptor. The result could be valuable knowing the capability of SLAM family receptors in binding to several morbilliviruses, such as the measles [55]. CD244/spike showed a different interaction pattern of SARS-CoV-2 RBD residues (G446, A475, G482, C488 and T500), though it has shared some common interacting amino acids (S477 and N481) from spike with the ACE2 receptor. Thus, the binding affinity of CD244/spike was slightly lower than ACE2/spike.

CD7 and CD4 from other SIgF members also showed promising results in the analysis for SARS-CoV-2 spike binding affinity. Despite of different binding mode, SARS-CoV-2 RBD could bind to CD7 and CD4 stronger (−15 and −13.3 kcal/mol, respectively) than ACE2/spike (−12.8 kcal/mol). CD4 as a co-receptor for MHC class II-restricted antigen-induced T cell activation and HIV receptor exists in T cells, innate lymphoid cells, monocytes, and macrophages [56]. CD7 as regulator of cytokine production and T cell activation is on the surface of T, NK cells and, thymocytes [57]. Recent studies reported reduction in T cells of COVID-19 cases [16,58,59]. Considering high binding affinity of CD4/spike could induce more curiosity to find the probable SARS-CoV-2 mechanism in avoiding T cell activation. However, negatively correlation of $CD4^+$ T cells and level of cytokines (TNF-α, IL-6) has suggested as the potential cause of T cell depletion in COVID-19 patients [23].

Other candidates that can be imagine for the virus binding are cell adhesion molecules (CAM) such as ICAM-1 or CD54 at the surface of lymphocytes, endothelial cells and fibroblasts that also, is receptor of Rhinoviruses [60], ICAM-2 or CD102 on the endothelial cells, ICAM-3 or CD50 on lymphocytes, ICAM-4 or CD242 on the majority of cells specially, erythrocytes and VCAM-1 or CD106 on the surface of macrophages, dendritic cells, endothelium [61]. The affinity of ICAMs and ACE2 in binding to SARS-CoV-2 RBD was relatively in the same range. Interestingly, CD54 showed similar binding affinity to SARS-CoV-2 RBD as well as VP1, VP2 and VP3 of Rhinoviruses. The results reinforce the need to pay more attention to the role of these receptors in interacting with SARS-CoV-2.

Other adhesion molecules that can be thought as receptors for the virus include CD56 or neural cell adhesion molecule (NCAM) [62], Neuropilin-1 (NRP1), and Basigin (BSG or CD147). The first, being present in NK and brain cells, the second in T cells and neurons and the third in pericytes, endothelial cells and leukocytes. Actually, experimental studies proved the NRP1 and BSG as receptors for the SARS-CoV-2 virus [63–66] and Meplazumab (CD147-specific humanized monoclonal antibody) as a therapeutic agent [67]. Interacting residues of SARS-CoV-2 RBD were various in binding to NCAM, BSG and NRP1, though the affinity of BSG and NRP1 to RBD was nearly similar. Consistent with the results of Ulrich et al. binding affinity and residues involved in the coronavirus RBD interactions highlighted CD147 as a target for COVID-19 treatment [68].

Chemokine receptors, in addition to their primary role in cellular chemotaxis, are also known as receptors for viruses. Amongst, CXCR6

Table 3
Molecular docking and Molecular dynamic simulation results of complexes.

Complexes	HADDOCK RMSD (Å)	Number of H-bonds from docking	Average number of H-bonds from MD	SASA (nm/S2/N)	RoG (nm)
CD26/RBD-spike	1.5	13	12	43	2.6
CD26/RBD-MERS	0.4	5	13	50	2.7
CD2/RBD-spike	0.8	17	9	44	2.85
CD56/RBD-spike	2.2	12	9	68	2.2
CD7/RBD-spike	1.8	11	10	38	2.4
CCR9/RBD-spike	0.8	13	10	43	3.0
CD150/RBD-spike	0.4	9	9	39	2.9
CD4/RBD-spike	0.4	11	10	38	2.5
CD50/RBD-spike	2.3	6	5	45	2.75
XCR1/RBD-spike	1.9	16	15	37	3.1
CD106/RBD-spike	1.2	15	14	36	2.5
ACE2/RBD-spike	1.5	13	14	65	2.8
CD54/RBD-spike	0.6	11	–	–	–
CD54/VP1	0.46	12	–	–	–
CD54/VP2	0.52	10	–	–	–
CD54/VP3	1.2	7	–	–	–
NRP1/RBD-spike	0.5	18	–	–	–
CD242/RBD-spike	2.6	9	–	–	–
CCR5/RBD-spike	2.0	8	–	–	–
CXCR6/RBD-spike	1.5	14	–	–	–
CD147/RBD-spike	1.7	8	–	–	–
CD102/RBD-spike	1.5	11	–	–	–
2B4/RBD-spike	1.7	7	–	–	–

(CD186), CCXCR1 (XCR1), CCR9 (CDw199), and CCR5 (CD195) that are expressed in a broad span of immune cells have shown the eligible interactions with spike of virus in docking analysis. A recent study reported that treatment with Leronlimab (CCR5 blocking antibody) have displayed restoration of immune system and a significant decrease in SARS-CoV-2 plasma viremia [69]. In the current study, relatively different interface of SARS-CoV-2 RBD was resulted in binding to CXCR6, XCR1, CCR9, and CCR5, although similar binding affinity was obtained in the CXCR6, XCR1, and CCR5 complex analysis (−12.4, −13.1 and −12.5 kcal/mol, respectively). The binding affinity of CCR9 complex was higher (−14.2 kcal/mol) compared to ACE2/spike.

Considering the importance of the structural behavior of protein-protein complexes, they were subjected to MD simulation to study the dynamic feature of a protein at atomic levels. MD provides insight into the conformational changes of proteins through time. RMSD, as the estimation of the average distance of a set of atoms in the input proteins for the same atoms during simulation, indicated the structural stability of complexes. Despite of various fluctuations, finally all complexes reached relatively steady state. The fluctuation pattern of the key residues of RBD-spike was approximately in the same range for all complexes, though CD26/MERS showed higher fluctuations compared to CD26/RBD-spike. The difference was consistent with the results of docking energy and binding affinity, where CD26/MERS complex showed smaller docking energy and Kd compared to CD26/RBD-spike and could be interpreted as the higher stability of CD26/RBD-spike. Further, the number of H-bonds in the interface of proteins and RBD-spike was remarkably comparable to the LigPlot analysis of complexes and could be considered as the stability of complexes during the simulation.

Besides of ACE2 diverse expression in many cell types also, the results of our study indicate extent of spike SARS-CoV-2 virus interaction with the mentioned receptors, which may be related to the broad range of clinical manifestations such as vasculitis (VCAM-1 on the endothelium), and neuro-olfactory disorders (NRP-1, NCAM, CD-147 on the neurocytes) [70,71]. Likewise, infection of the immune cells with the SARS-CoV-2 virus can be important because they may be served as a "Trojan horse" to spread the virus throughout the human body.

The importance of the reduction of T Cells in COVID-19 is determined by the fact that despite of the antibody response and cytokines production by other immune cells in severe patients, they often have trouble in management of SARS-CoV-2, permitting the virus to proliferate in high levels. The innate immune cells respond by secreting still more cytokines and cause cytokine storm [72,73]. Furthermore, for effective antibody responses, bilateral cooperation of T and B lymphocytes in the germinal centers of the lymphatic tissue is required [74]. B cells within germinal centers shuffle Immunoglobulin (Ig) genes via somatic hyper mutation and generate Ig variants which afterward contend for T follicular helper (TFH) cell survival signal and as a result, B cells that generating low affinity and auto-reactive antibodies are omitted. This process promotes the affinity maturation of the antibodies generated by the B cells and facilitates differentiation of these B cells into plasma and memory B cells, essential cell types for durable antibody production, and impressive humoral immune responses [75,76]. Accordingly, the lack of functional T Cells has resulted in appearance of antibodies that are not neutralizing the virus and cannot prevent the progression of the disease or react against their self-cells. This mechanism is important because in the etiology of COVID-19 has shown that auto-antibodies, by attacking the blood vessels, cause clots, which ultimately leads to impaired blood flow and stroke. Overall, the affinity of several immune receptor candidates in binding to SARS-CoV-2 RBD was evaluated aiming to highlight potential roles in association with COVID-19. Further studies and experiments can improve the results of this research.

5. Conclusion

Considerable reduction of lymphocytes, monocytes, basophils, and dendritic cells in severe and moderate SARS-CoV-2 infections induced us to evaluate the immune receptors that may be potentially involved in virus entry. The higher binding affinity of several immune receptors to the SARS-CoV-2 RBD compared to ACE2 can justify the aim of the study to consider other receptors as therapeutic targets for meeting the challenge of COVID-19.

Author contributions were as following

Conception and design the study: Saeed Mobini, Milad Chizari, Elham Rismani.

Collection, analysis of data and writing assistance: Saeed Mobini, Milad Chizari, Ladan Mafakher, Elmira Rismani, Elham Rismani.

Final approval of manuscript: Elham Rismani, Saeed Mobini, Milad Chizari.

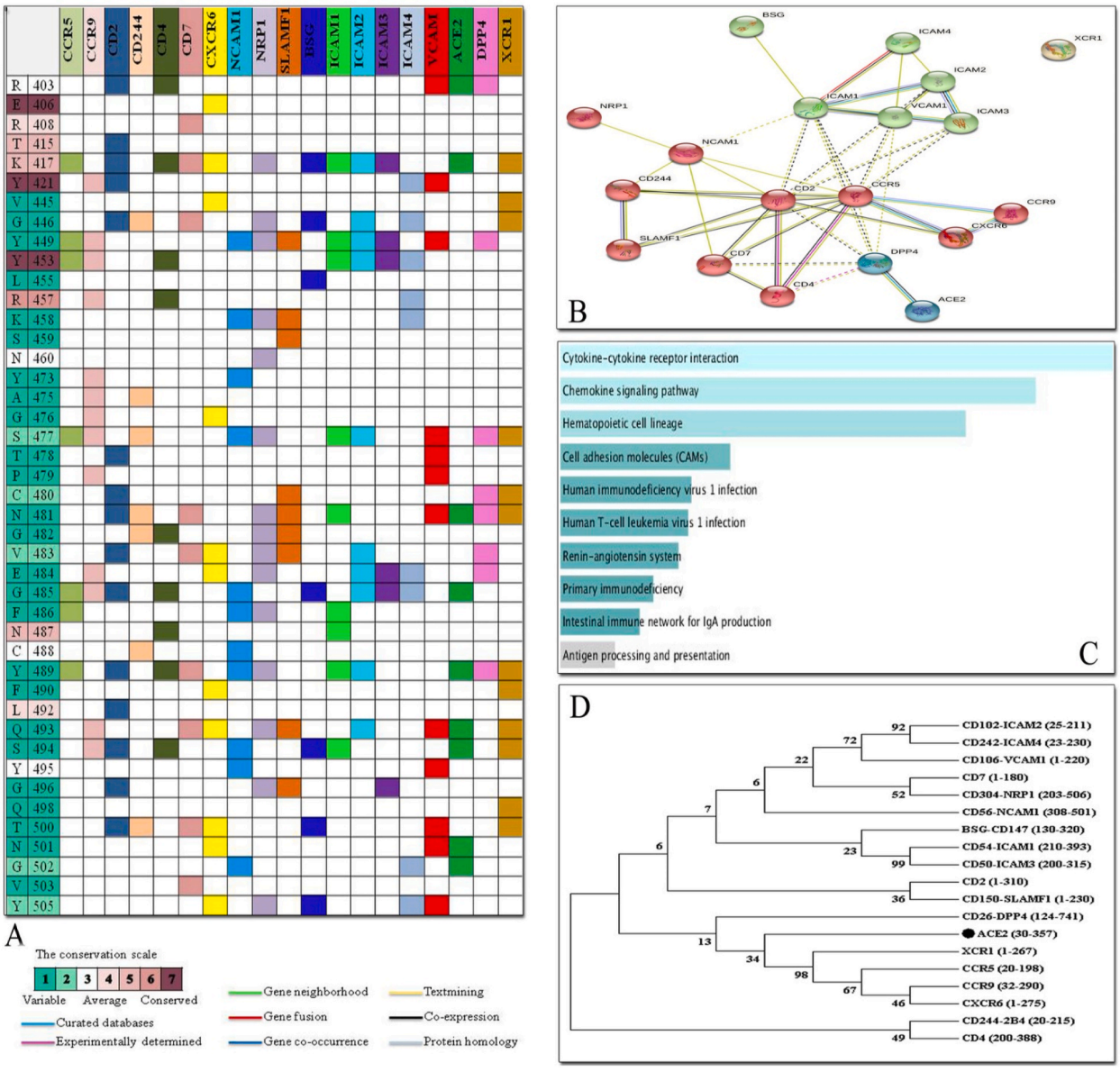

Fig. 12. Interaction map of the RBD domain of SARS-Cov-2 spike into receptors as well as PPI network analysis. A) Interacting residues on the basis of molecular docking results as well as conservation grade of residues of the RBD domain of spike. B) STRING PPI network of human proteins. C) Enrichment pathway analysis of PPI network in KEGG. D) Phylogenetic tree of protein sequences using Neighbor Joining method with bootstrapping to provide confidence for tree topology. The percentage of replicate trees in which the associated taxa clustered together in the bootstrap values (1000 replicates) has been depicted next to the branches.

Declaration of competing interest

The authors declare that they have no known competing financial interests or personal relationships that could have appeared to influence the work reported in this paper.

Acknowledgements

None.

References

[1] I. Astuti, Severe Acute Respiratory Syndrome Coronavirus 2 (SARS-CoV-2): an overview of viral structure and host response, Diabetes & Metabolic Syndrome: Clin. Res. Rev. 14 (4) (2020) 407–412.
[2] K.G. Andersen, A. Rambaut, W.I. Lipkin, E.C. Holmes, R.F. Garry, The proximal origin of SARS-CoV-2, Nat. Med. 26 (4) (2020) 450–452.
[3] B. Korber, W.M. Fischer, S. Gnanakaran, H. Yoon, J. Theiler, W. Abfalterer, et al., Tracking changes in SARS-CoV-2 Spike: evidence that D614G increases infectivity of the COVID-19 virus, Cell 182 (4) (2020) 812–827, e19.
[4] H. Tegally, E. Wilkinson, M. Giovanetti, A. Iranzadeh, V. Fonseca, J. Giandhari, et al., Emergence and rapid spread of a new severe acute respiratory syndrome-related coronavirus 2 (SARS-CoV-2) lineage with multiple spike mutations in South Africa, medRxiv (2020), 2020.12.21.20248640..
[5] J. Wise, Covid-19: New Coronavirus Variant Is Identified in UK. British Medical Journal Publishing Group, 2020.
[6] M. Marsh, A. Helenius, Virus entry: open sesame, Cell 124 (4) (2006) 729–740.
[7] J. Mercer, M. Schelhaas, A. Helenius, Virus entry by endocytosis, Annu. Rev. Biochem. 79 (2010) 803–833.
[8] T.M. Clausen, D.R. Sandoval, C.B. Spliid, J. Pihl, H.R. Perrett, C.D. Painter, et al., SARS-CoV-2 infection depends on cellular heparan sulfate and ACE2, Cell 183 (4) (2020) 1043–1057.e15.
[9] L. Suprewicz, M. Swoger, S. Gupta, E. Piktel, F.F. Byfield, D.V. Iwamoto, et al., Vimentin Binds to SARS-CoV-2 Spike Protein and Antibodies Targeting Extracellular Vimentin Block in Vitro Uptake of SARS-CoV-2 Virus-like Particles. bioRxiv, 2021, 01. 08.425793.

[10] Q. Wang, Y. Zhang, L. Wu, S. Niu, C. Song, Z. Zhang, et al., Structural and functional basis of SARS-CoV-2 entry by using human ACE2, Cell 181 (4) (2020) 894–904.e9.

[11] M. Hoffmann, H. Kleine-Weber, S. Schroeder, N. Krüger, T. Herrler, S. Erichsen, et al., SARS-CoV-2 cell entry depends on ACE2 and TMPRSS2 and is blocked by a clinically proven protease inhibitor, Cell 181 (2) (2020) 271–280.e8.

[12] I. Hamming, W. Timens, M. Bulthuis, A. Lely, Navis Gv, H. van Goor, Tissue distribution of ACE2 protein, the functional receptor for SARS coronavirus. A first step in understanding SARS pathogenesis, J. Pathol.: J. Pathol. Soc. Great Britain and Ireland 203 (2) (2004) 631–637.

[13] N. Vabret, G.J. Britton, C. Gruber, S. Hegde, J. Kim, M. Kuksin, et al., Immunology of COVID-19: current state of the science, Immunity 52 (6) (2020) 910–941.

[14] L. Yang, S. Liu, J. Liu, Z. Zhang, X. Wan, B. Huang, et al., COVID-19: immunopathogenesis and Immunotherapeutics, Signal Transduction and Targeted Therapy 5 (1) (2020) 1–8.

[15] R. Zhou, K.K.-W. To, Y.-C. Wong, L. Liu, B. Zhou, X. Li, et al., Acute SARS-CoV-2 infection impairs dendritic cell and T cell responses, Immunity 53 (4) (2020) 864–877.e5.

[16] G. Chen, D. Wu, W. Guo, Y. Cao, D. Huang, H. Wang, et al., Clinical and immunological features of severe and moderate coronavirus disease 2019, J. Clin. Invest. (5) (2020) 130.

[17] D.M. Del Valle, S. Kim-Schulze, H.-H. Huang, N.D. Beckmann, S. Nirenberg, B. Wang, et al., An inflammatory cytokine signature predicts COVID-19 severity and survival, Nat. Med. 26 (10) (2020) 1636–1643.

[18] D. Weiskopf, K.S. Schmitz, M.P. Raadsen, A. Grifoni, N.M. Okba, H. Endeman, et al., Phenotype of SARS-CoV-2-specific T-cells in COVID-19 patients with acute respiratory distress syndrome, medRxiv 5 (48) (2020) eabd2071.

[19] A.K. Azkur, M. Akdis, D. Azkur, M. Sokolowska, W. van de Veen, M.C. Brüggen, et al., Immune response to SARS-CoV-2 and mechanisms of immunopathological changes in COVID-19, Allergy 75 (7) (2020) 1564–1581.

[20] L.A. Huppert, M.A. Matthay, L.B. Ware (Eds.), Pathogenesis of Acute Respiratory Distress Syndrome. Seminars in Respiratory and Critical Care Medicine, 2019. NIH Public Access.

[21] M. Sokolowska, Z.M. Lukasik, I. Agache, C.A. Akdis, D. Akdis, M. Akdis, et al., Immunology of COVID-19: mechanisms, clinical outcome, diagnostics, and perspectives—a report of the European academy of allergy and clinical immunology (EAACI), Allergy 75 (10) (2020) 2445–2476.

[22] C. Qin, L. Zhou, Z. Hu, S. Zhang, S. Yang, Y. Tao, et al., Dysregulation of immune response in patients with COVID-19 in Wuhan, China, Clin. Infect. Dis. 71 (15) (2020) 762–768.

[23] B. Diao, C. Wang, Y. Tan, X. Chen, Y. Liu, L. Ning, et al., Reduction and functional exhaustion of T cells in patients with coronavirus disease 2019 (COVID-19), Front. Immunol. 11 (2020) 827.

[24] H. Chu, J. Zhou, B.H.-Y. Wong, C. Li, J.F.-W. Chan, Z.-S. Cheng, et al., Middle East respiratory syndrome coronavirus efficiently infects human primary T lymphocytes and activates the extrinsic and intrinsic apoptosis pathways, J. Infect. Dis. 213 (6) (2016) 904–914.

[25] J.-M. Kim, Y.-S. Chung, H.J. Jo, N.-J. Lee, M.S. Kim, S.H. Woo, et al., Identification of coronavirus isolated from a patient in korea with COVID-19, Osong public health and research perspectives 11 (1) (2020) 3.

[26] X. Wang, W. Xu, G. Hu, S. Xia, Z. Sun, Z. Liu, et al., SARS-CoV-2 infects T lymphocytes through its spike protein-mediated membrane fusion, Cell. Mol. Immunol. (2020) 1–3.

[27] J. Söding, Protein homology detection by HMM–HMM comparison, Bioinformatics 21 (7) (2005) 951–960.

[28] A. Roy, A. Kucukural, Y. Zhang, I-TASSER: a unified platform for automated protein structure and function prediction, Nat. Protoc. 5 (4) (2010) 725–738.

[29] R.A. Laskowski, M.W. MacArthur, D.S. Moss, J.M. Thornton, PROCHECK: a program to check the stereochemical quality of protein structures, J. Appl. Crystallogr. 26 (2) (1993) 283–291.

[30] M. Wiederstein, M.J. Sippl, ProSA-web: interactive web service for the recognition of errors in three-dimensional structures of proteins, Nucleic Acids Res. 35 (suppl_2) (2007) W407–W410.

[31] G. Celniker, G. Nimrod, H. Ashkenazy, F. Glaser, E. Martz, I. Mayrose, et al., ConSurf: using evolutionary data to raise testable hypotheses about protein function, Isr. J. Chem. 53 (3–4) (2013) 199–206.

[32] F. Glaser, T. Pupko, I. Paz, R.E. Bell, D. Bechor-Shental, E. Martz, et al., ConSurf: identification of functional regions in proteins by surface-mapping of phylogenetic information, Bioinformatics 19 (1) (2003) 163–164.

[33] G. Van Zundert, J. Rodrigues, M. Trellet, C. Schmitz, P. Kastritis, E. Karaca, et al., The HADDOCK2. 2 web server: user-friendly integrative modeling of biomolecular complexes, J. Mol. Biol. 428 (4) (2016) 720–725.

[34] D. Kozakov, D.R. Hall, B. Xia, K.A. Porter, D. Padhorny, C. Yueh, et al., The ClusPro web server for protein-protein docking, Nat. Protoc. 12 (2) (2017) 255–278.

[35] S.J. de Vries, A.M. Bonvin, CPORT: a consensus interface predictor and its performance in prediction-driven docking with HADDOCK, PloS One 6 (3) (2011), e17695.

[36] W.L. DeLano, The pymol molecular graphics system, 2002, http://www.pymol.org, 2002.

[37] R.A. Laskowski, M.B. Swindells, LigPlot+: multiple ligand–protein interaction diagrams for drug discovery, ACS Publications 51 (10) (2011) 2778–2786.

[38] L.C. Xue, J.P. Rodrigues, P.L. Kastritis, A.M. Bonvin, A. Vangone, PRODIGY: a web server for predicting the binding affinity of protein–protein complexes, Bioinformatics 32 (23) (2016) 3676–3678.

[39] M.J. Abraham, T. Murtola, R. Schulz, S. Páll, J.C. Smith, B. Hess, et al., GROMACS: high performance molecular simulations through multi-level parallelism from laptops to supercomputers, Software 2015/09/01/ (1–2) (2015) 19–25.

[40] E.Y. Chen, C.M. Tan, Y. Kou, Q. Duan, Z. Wang, G.V. Meirelles, et al., Enrichr: interactive and collaborative HTML5 gene list enrichment analysis tool, BMC Bioinf. 14 (1) (2013) 128.

[41] D. Szklarczyk, A.L. Gable, D. Lyon, A. Junge, S. Wyder, J. Huerta-Cepas, et al., STRING v11: protein–protein association networks with increased coverage, supporting functional discovery in genome-wide experimental datasets, Nucleic Acids Res. 47 (D1) (2019) D607–D613.

[42] F. Sievers, D.G. Higgins, Clustal Omega, Accurate Alignment of Very Large Numbers of Sequences. Multiple Sequence Alignment Methods: Springer, 2014, pp. 105–116.

[43] S. Kumar, G. Stecher, K. Tamura, MEGA7: molecular evolutionary genetics analysis version 7.0 for bigger datasets, Mol. Biol. Evol. 33 (7) (2016) 1870–1874.

[44] M. Borsa, J.M. Mazet, Attacking the defence: SARS-CoV-2 can infect immune cells, Nat. Rev. Immunol. 20 (10) (2020) 1–10, 1-.

[45] A.N. Jain, Bias, reporting, and sharing: computational evaluations of docking methods, J. Comput. Aided Mol. Des. 22 (3–4) (2008 Mar-Apr) 201–212.

[46] T. Ishii, K. Ohnuma, A. Murakami, N. Takasawa, S. Kobayashi, N.H. Dang, et al., CD26-mediated signaling for T cell activation occurs in lipid rafts through its association with CD45RO, Proc. Natl. Acad. Sci. Unit. States Am. 98 (21) (2001) 12138–12143.

[47] T. Tanaka, J. Kameoka, A. Yaron, S.F. Schlossman, C. Morimoto, The costimulatory activity of the CD26 antigen requires dipeptidyl peptidase IV enzymatic activity, Proc. Natl. Acad. Sci. Unit. States Am. 90 (10) (1993) 4586–4590.

[48] Y. Torimoto, N. Dang, E. Vivier, T. Tanaka, S. Schlossman, C. Morimoto, Coassociation of CD26 (dipeptidyl peptidase IV) with CD45 on the surface of human T lymphocytes, J. Immunol. 147 (8) (1991) 2514–2517.

[49] Y. Li, Z. Zhang, L. Yang, X. Lian, Y. Xie, S. Li, et al., The MERS-CoV receptor DPP4 as a candidate binding target of the SARS-CoV-2 spike, Iscience (2020) 101160.

[50] Wang J-h, Protein recognition by cell surface receptors: physiological receptors versus virus interactions, Trends Biochem. Sci. 27 (3) (2002) 122–126.

[51] A.M. Krensky, F. Sanchez-Madrid, E. Robbins, J.A. Nagy, T.A. Springer, S. J. Burakoff, The functional significance, distribution, and structure of LFA-1, LFA-2, and LFA-3: cell surface antigens associated with CTL-target interactions, J. Immunol. 131 (2) (1983) 611–616.

[52] P. Selvaraj, M.L. Plunkett, M. Dustin, M.E. Sanders, S. Shaw, T.A. Springer, The T lymphocyte glycoprotein CD2 binds the cell surface ligand LFA-3, Nature 326 (6111) (1987) 400–403.

[53] H. Pahima, P.G. Puzzovio, F. Levi-Schaffer, 2B4 and CD48: a powerful couple of the immune system, Clin. Immunol. 204 (2019) 64–68.

[54] N. Wu, A. Veillette, SLAM family receptors in normal immunity and immune pathologies, Curr. Opin. Immunol. 38 (2016) 45–51.

[55] M.A. Dragovich, A. Mor, The SLAM family receptors: potential therapeutic targets for inflammatory and autoimmune diseases, Autoimmunity Reviews 17 (7) (2018) 674–682, 2018/07/01.

[56] R.R. Rich, T.A. Fleisher, W.T. Shearer, H.W. Schroeder Jr., A.J. Frew, C. M. Weyand, Clinical Immunology E-Book: Principles and Practice, Elsevier Health Sciences, 2012.

[57] C.A. Janeway Jr., Immunobiology, 2020.

[58] D. Wang, B. Hu, C. Hu, F. Zhu, X. Liu, J. Zhang, et al., Clinical characteristics of 138 hospitalized patients with 2019 novel coronavirus–infected pneumonia in Wuhan, China, Jama 323 (11) (2020) 1061–1069.

[59] C. Huang, Y. Wang, X. Li, L. Ren, J. Zhao, Y. Hu, et al., Clinical features of patients infected with 2019 novel coronavirus in Wuhan, China, The lancet 395 (10223) (2020) 497–506.

[60] J. Grove, M. Marsh, The cell biology of receptor-mediated virus entry, JCB (J. Cell Biol.) 195 (7) (2011) 1071–1082.

[61] J. Chihara, Immunoglobulin super family (ICAM, VCAM, NCAM), Nihon rinsho Japanese journal of clinical medicine 63 (2005) 139.

[62] H.H. Van Acker, A. Capsomidis, E.L. Smits, V.F. Van Tendeloo, CD56 in the immune system: more than a marker for cytotoxicity? Front. Immunol. 8 (2017) 892.

[63] L. Cantuti-Castelvetri, R. Ojha, L.D. Pedro, M. Djannatian, J. Franz, S. Kuivanen, et al., Neuropilin-1 facilitates SARS-CoV-2 cell entry and provides a possible pathway into the central nervous system, bioRxiv 370 (6518) (2020) 856–860.

[64] J.L. Daly, B. Simonetti, C.A. Plagaro, M.K. Williamson, D.K. Shoemark, L. Simon-Gracia, et al., Neuropilin-1 is a host factor for SARS-CoV-2 infection, bioRxiv 370 (6518) (2020) 861–865.

[65] C. Iadecola, J. Anrather, H. Kamel, Effects of COVID-19 on the nervous system, Cell 183 (1) (2020) 16–27.e1.

[66] K. Wang, W. Chen, Y.-S. Zhou, J.-Q. Lian, Z. Zhang, P. Du, et al., SARS-CoV-2 invades host cells via a novel route: CD147-spike protein, BioRxiv (2020), https://doi.org/10.1101/2020.03.14.988345.

[67] H. Bian, Z.-H. Zheng, D. Wei, Z. Zhang, W.-Z. Kang, C.-Q. Hao, et al., Meplazumab treats COVID-19 pneumonia: an open-labelled, concurrent controlled add-on clinical trial, MedRxiv (2020), https://doi.org/10.1101/2020.03.21.20040691, 2020.03.21.20040691.

[68] H. Ulrich, M. Pillat, CD147 as a target for COVID-19 treatment: suggested effects of azithromycin and stem cell engagement, Stem Cell Reviews and Reports 16 (3) (2020) 434–440.

[69] B.K. Patterson, H. Seethamraju, K. Dhody, M.J. Corley, K. Kazempour, J.P. Lalezari, et al., Disruption of the CCL5/RANTES-CCR5 pathway restores immune homeostasis and reduces plasma viral load in critical COVID-19, medRxiv : the preprint server for health sciences (2020), 2020.05.02.20084673.

[70] M. Heming, X. Li, S. Räuber, A.K. Mausberg, A.-L. Börsch, M. Hartlehnert, et al., Neurological manifestations of COVID-19 feature T cell exhaustion and dedifferentiated monocytes in cerebrospinal fluid, Immunity 54 (1) (2020) 164–175.e6.
[71] M.-H. Lee, D.P. Perl, G. Nair, W. Li, D. Maric, H. Murray, et al., Microvascular injury in the brains of patients with covid-19, N. Engl. J. Med. 384 (5) (2020) 481–483.
[72] N. Taefehshokr, S. Taefehshokr, N. Hemmat, B. Heit, Covid-19: perspectives on innate immune evasion, Front. Immunol. (2020) 11.
[73] Q. Ye, B. Wang, J. Mao, The pathogenesis and treatment of theCytokine Storm'in COVID-19, J. Infect. 80 (6) (2020) 607–613.
[74] Y. Chen, A. Zuiani, S. Fischinger, J. Mullur, C. Atyeo, M. Travers, et al., Quick COVID-19 healers sustain anti-SARS-CoV-2 antibody production, Cell 183 (6) (2020) 1496–1507.e16.
[75] J.G. Cyster, C.D. Allen, B cell responses: cell interaction dynamics and decisions, Cell 177 (3) (2019) 524–540.
[76] L. Mesin, J. Ersching, G.D. Victora, Germinal center B cell dynamics, Immunity 45 (3) (2016) 471–482.